NASA TM 77480

NASA-TM-77480 19880017231

NASA TECHNICAL MEMORANDUM

TM 77480

EXPERIMENTAL INVESTIGATION OF THE TURBULENT FLOW IN SMOOTH AND LONGITUDINAL GROOVED TUBES

P. Nitschke

Translation of "Experimentelle Undersuchung der turbulenten Stroemung in glatten und laengsgerillten Rohren," Max-Planck Institue fuer Stromungsforschung, Goettingen, West Germany, 1983.

NATIONAL AERONAUTICS AND SPACE ADMINISTRATION

WASHINGTON, D.C. 20546, May 1984

STANDARD TITLE PAGE

1. Report No. NASA TM77480	2. Government Accession No.	3. Recipient's Catalog No.
4. Title and Subtitle EXPERIMENTAL INVESTIGATION OF TURBULENT FLOW IN SMOOTH & LONGITUDINAL GROOVED TUBES		5. Report Date 6. Performing Organization Code
7. Author(s) P. Nitschke		8. Performing Organization Report No. 10. Work Unit No.
9. Performing Organization Name and Address Leo Kanner Assoc. Redwood City, CA.		11. Contract or Grant No. NASw 3541 13. Type of Report and Period Covered Translation
12. Sponsoring Agency Name and Address		14. Sponsoring Agency Code

15. Supplementary Notes

Experimentelle Untersuchung der turbulent Stroemung in glatten und laengsgerillten Rohren, Max-Planck Institut fuer Stromungsforschung, Goettingen, West Germany, 1983

16. Abstract

See attached.

17. Key Words (Selected by Author(s))	18. Distribution Statement		
	Unclassified - Unlimited		
19. Security Classif. (of this report) Unclassified	20. Security Classif. (of this page) Unclassified	21. No. of Pages	22.

N-154,666
N84-16510# CORRECTION
N88-26615#

Translation of title:

Experimental investigation of the turbulent flow in smooth and longitudinal grooved tubes

Abstract:

This report gives a short survey of an investigation of W. E. Reif. He discovered that shark-scales have fine grooves (characteristic breadth: 0. 1 mm) making a sort of streamline pattern on the shark's body. As a result, both of this investigation, and of some other works on structures in a turbulent boundary layer, in the Max-Planck-Institut für Strömungsforschung a model has been developed, which leads to the expectation, that grooves on a surface reduce the momentum exchange, and thus the drag of this surface compared to that of a smooth surface. To test this thesis, drag law, velocity profile and the profile of the velocity fluctuation were determined for tubes both, with and without longitudinal grooves. A comparison of these results shows, that for moderate Reynolds numbers ($8000 < Re_D < 45000$) the drag coefficient λ measured for the grooved tubes is about 3 % smaller than that of the smooth tubes. At higher Reynolds numbers, however, the drag coefficient for grooved tubes becomes larger than that for smooth tubes. For the above range of moderate Reynolds numbers the dimensionless breath of the grooves $b^+ = b \frac{u\tau}{\nu}$ lies between 8 and 30, thus having the same order of magnitude as that, calculated for the grooves on the shark-scales. No significant differences in the velocity profiles between grooved tubes and smooth tubes have been found. This, however, may be due to the comparitively bad spatial resolution of the hot-wire used here.

CONTENTS

		Page
List of Symbols		
1.	Introduction	1
2.	Fundamental Considerations	2
2.1	General Information on the Flow Resistance of Rough Walls	2
2.2	Comments on the Grooves on the Scales of the Shark	2
2.3	Model Conceptions of the Influence of Grooves on Longitudinal Structures in Near-Wall Turbulent Flow	7
3.	Test Set-up	8
3.1	Tube Channel	8
3.2	Tubes	11
3.3	Pressure Holes	13
3.4	Electronic Section	15
4.	Flow Resistance of the Investigated Tubes	16
4.1	General Fundamentals on the Resistance Law	16
4.2	Measurement Methods and Accuracy	19
4.2.1	Measurement of the Flow-Through	19
4.2.2	Determination and Accuracy of the Average Pressure Drop	20
4.2.3	Measurement of Diameter and Its Definition for Grooved Tubes	28
4.2.4	Determination of the Density and Kinematic Viscosity	30
4.3	Measurement Accuracy for the Coefficient of Resistance λ and the Reynolds Number Re	30
4.4	Results and Discussion	31
4.4.1	Smooth Tubes	31
4.4.2	Grooved Tubes	34
5.	Profile of Average Velocity $\bar{u}$ and of the Effective Value of the Velocity Fluctuations u'_{rms}	40
5.1	Introduction	40
5.2	Measurement Method and Accuracy	43

		Page
5.3	Results and Discussion	47
5.3.1	Smooth Tubes	47
5.3.2	Grooved Tubes	56
6.	Summary and Discussion of Future Work	66
7.	References	67

List of Symbols

$\varkappa$	Proportionality constant between mixing path and wall separation
λ	Coefficient of resistance
μ	Dynamic viscosity
ν	Kinematic viscosity
ϱ	Density
τ	Shear Stress
τ_w	Wall shear stress
τ_B	Wall shear stress over the groove crest
τ_T	Wall shear stress over the groove valley
A	Cross-sectional area between two grooves of the grooved tube
a	Position on the micrometer screw
b	Spacing of groove crests
$b^+ = b \cdot \frac{u_\tau}{\nu}$	Dimensionless spacing of groove crests
C	Integration constant
d	Diameter of the tube
f	General function
h	Groove height, roughness height
$h^+ = h \cdot \frac{u_\tau}{\nu}$	Dimensionless groove height
i	Continuous numbering of pressure holes
l	Various lengths
n	Exponent

p	Pressure (generally pressure difference compared to atmospheric pressure)
p_{iA} p_{iB}	Pressure at drill hole i = 1 - 9 Side A or B, respectively
p_o	Atmospheric pressure
p_{DDM}	Over-pressure in the spin flowmeter (DDM)
Q	Flow-through
q	Stagnation pressure
r	Radius, r_I, r_H, r_F, r_A see figure 4/9
Re	Reynolds number
u	Velocity in the flow direction, $u = \bar{u} + u'$
$\bar{u}$	Average local velocity in the flow direction
u_M	$\bar{u}$ in the tube middle
u'	Alternate component of u
$u'_{rms} = \sqrt{\overline{u'^2}}$	Effective value of the alternate component in flow direction
$u_Q = \frac{Q}{\pi r^2}$	Average velocity
$u_\tau = \sqrt{\frac{\tau_w}{\rho}}$	Wall velocity of shear stress
$u^+ = \frac{\bar{u}}{u_\tau}$	Dimensionless average local velocity
ΔW	Change in Resistance
x	Tube longitude coordinate in flow direction, x=0: Tube front
y	Wall separation coordinate, y = 0: Wall contact
$y^+ = y \cdot \frac{u_\tau}{\nu}$	Dimensionless wall separation
z	Coordinate perpendicular to x and y, i.e. perpendicular to the flow direction and parallel to the wall
$z^+ = z \cdot \frac{u_\tau}{\nu}$	Dimensionless coordinate perpendicular to x and y

1. Introduction

The reduction of flow resistance is one of the most important research tasks in the area of flow research. In addition to shaping objects exposed to the flow, the structure of the surface plays an important role in the occurring energy losses. For this reason, numerous investigations have been conducted on the flow resistance of smooth and rough surfaces (e.g. Nikuradse 1933, Hopf 1923, Fromm 1923, Schlichting 1936, Wieghardt 1943). These investigations show that the smooth wall has the smallest flow resistance, compared to all investigated roughnesses. Proceeding from these results it is assumed that the smooth wall in general offers the lowest flow resistance compared to any other surface structure.

Various observations do indicate however, that this assumption should be re-examined. Investigations by Reif showed for example, that the scales of sharks are covered with fine, longitudinal grooves. The scales overall produce a type of flow-line configuration on the fish (Reif 1978). According to model conceptions developed by Dinkelacker (Reif and Dinkelacker 1981), these grooves can affect the flow so much that longitudinal structures are generated which are smaller than those observed on smooth walls. This diminution could reduce the pulse exchange near the wall and thus reduce the friction resistance.

It is the goal of this paper to investigate whether the resistance and the effective value of the velocity fluctuations change due to a longitudinal-grooved surface and whether this change exhibits any dependence on the Reynolds number and on the groove width $b^+ = b \frac{u_\tau}{\nu}$ made dimensionless by the flow quantities u_τ and ν. The mechanism by which the grooves exert their potential influence will be of secondary importance. As flow form, the flow in a tube was chosen, due to the simple geometry and the easily measured flow resistance. In the first part of the investigation, the resistance law will be compared on smooth tubes and tubes with longitudinal grooves. In the second part of the investigation, velocity profiles and profiles of the effective value of the velocity fluctuations in the flow direction will be compared for smooth and grooved tubes and the results will be related to other measurements.

2. Fundamental Considerations

2.1 General Information on the Flow Resistance on Rough Walls

There are numerous investigations on the friction losses from rough walls; these cover a broad range of Reynolds numbers and were conducted on very different roughnesses, like sand, geometric elements in regular and irregular arrangement, wall holes etc. (Nikuradse 1933, Schlichting 1936, Wieghardt 1943). Nikuradse investigated the sand roughness in great detail; its tube walls in this case were packed as tightly as possible with sand grains of the same, defined size. According to these measurements and according to discussions by Prandtl (Schlichting 1965, p. 573), there are three different regions in which the friction resistance can be variously affected. The decisive parameter is the roughness height $h^+ = h \cdot \frac{u_\tau}{\nu}$ made dimensionless by the characteristic length of the viscous under-layer $\frac{\nu}{u_\tau}$. If h^+ is less than 5, then the roughness has no measurable influence on the resistance, since the roughness disappears entirely in the viscous under-layer which was formerly viewed as a laminar under-layer. If h^+ lies between 5 and 70, then the resistance is also dependent on the Reynolds number and on h^+. In the third region, $h^+ > 70$, the influence of h^+ exceeds that of the Reynolds number, so that the resistance depends only on h^+ and is very much greater than that of the smooth wall. According to measurements by Schlichting (1936), a random roughness, e.g. less densely packed sand grains or roughnesses in the shape of spheres, hemispheres, cones etc., can be assigned an equivalent sand roughness and applied in this manner to the relationships found by Nikuradse.

All these roughnesses have in common that they increase the resistance of the overflowed surface essentially by means of two mechanisms (Prandtl 1969, p. 191, Rotta 1972, p. 159). Due to the resistance of the shape, an additional pressure loss occurs in the flow. At the enlarged surface, due to additional, viscous friction, the near-wall velocity profile and thus the wall shear stress $\tau_w = \mu \left.\frac{d\bar{u}}{dy}\right|_{y=0}$ changes. In general this thesis states that a smooth wall exposes the flow to the smallest resistance. Investigations in biology and new findings on coherent structures in turbulent flow provide an impetus to rethink this thesis.

2.2 Comments on the Grooves on the Scales of the Shark

According to observations by Reif (Reif 1978), scales of several very-fast swimming sharks are covered with longitudinal grooves. The photos 2/1 to 2/7 show several examples which were also prepared by Reif (personal report). Figure 2/1 presents a larger section of the skin surface of a hammerhead shark. The grooves running uniformly over the skin are clearly seen on the indistinct scales. In the middle of the photo there is pit-organ, probably a sensory organ, whose function is still unexplained.

It is striking that the grooves run toward this pit. Figure 2/8 shows a shark with the run of the grooves represented by arrows. The dotted surfaces indicate flat scales without grooves. The overall impression resembles the flow line picture of a flow about the body of the shark.

Figure 2/2 shows the scales of the velvet shark (highly enlarged). Again, in the middle of the photo we see the pit organ toward which the grooves run. In contrast to this, the grooves in fig. 2/3 run around the collateral line organ which approximately corresponds to the human ear.

Figure 2/4 shows the skin in the tail region near the stagnation edge. We clearly see the very minutely formed grooves here.

As we see in figure 2/5, the scales of embryos are also provided with grooves.

There seems to be a close relationship between the formation of the grooves and the flow:

-shape of the flow line of the groove pattern
-convergence of grooves to the pit organ, divergence of grooves before a collateral line organ
-low groove depth near the stagnation edges, e.g. front edge of fins where the boundary layer is still quite thin
-unchanged grooves in the course of development of the shark (see also Reif, Dinkelacker 1981).

Figures 2/6 and 2/7 indicate the shape of the grooves: Narrow, peaked "crests" and definitely round "valleys." Measurements by Reif showed a distance b of groove crests of between 40 and 105 μm, an average value of 60 μm and a ratio of groove height h to groove separation b of 1:2 to 1:3. In order to be able to norm these quantities with the characteristic length of the viscous underlayer $\frac{\nu}{u_\tau}$ several assumptions must be made since the velocity of wall shear stress u_τ for the shark is not known. In an initial estimation, the flow around the shark can be compared with the conditions of a plate exposed to a flow at a speed u_∞, so that we have:

$$u_\tau \approx 0{,}04\, u_\infty$$

With a temperature of T = 20 °C and a kinematic viscosity of $\nu = 10^{-6} m^2/s$ the values given in table 2/1 result for the dimensionless groove width $b^+ = b \cdot \frac{u_\tau}{\nu}$ and the dimensionless groove height $h^+ = h \cdot \frac{u_\tau}{\nu}$ for three streaming velocities between 5 m/s and 20 m/s.

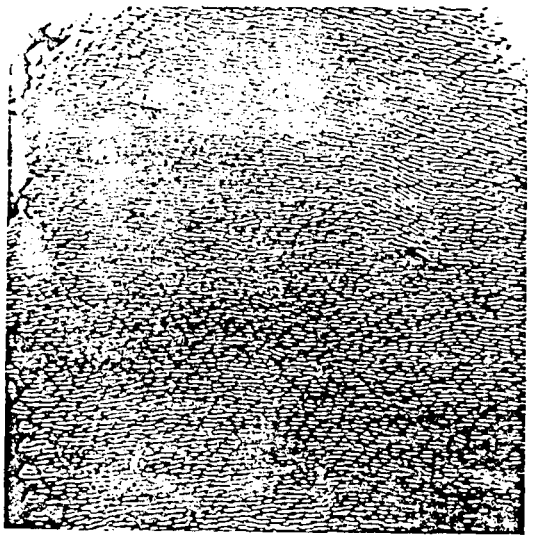

Fig. 2/1: Section of Surface Skin from Hammerhead Shark with Pit Organ (Adult, 1.02 m long, 12x enlargement)

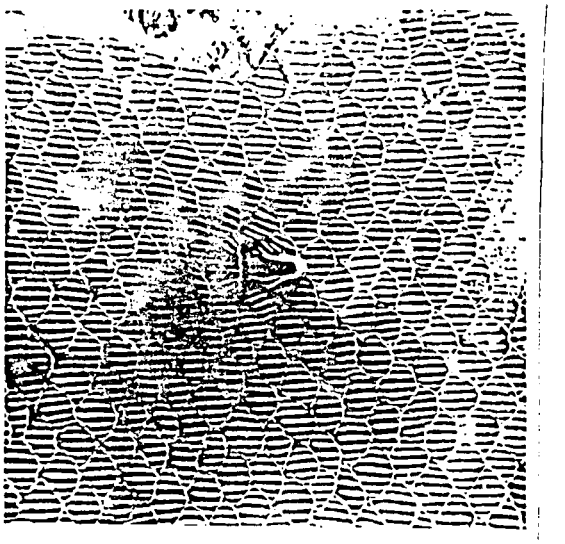

Fig. 2/2: Grooved Fins of the Velvet Shark, Pit Organ in Middle (Adult, 2.80 m long, 20x enlargement)

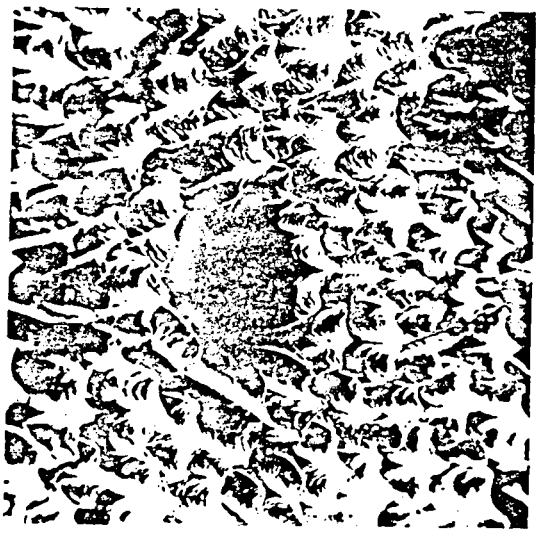

Fig. 2/3: Grooves Running around the Collateral Line organ of the Blueshark (Adult, 2.34 m long, 60x enlargement)

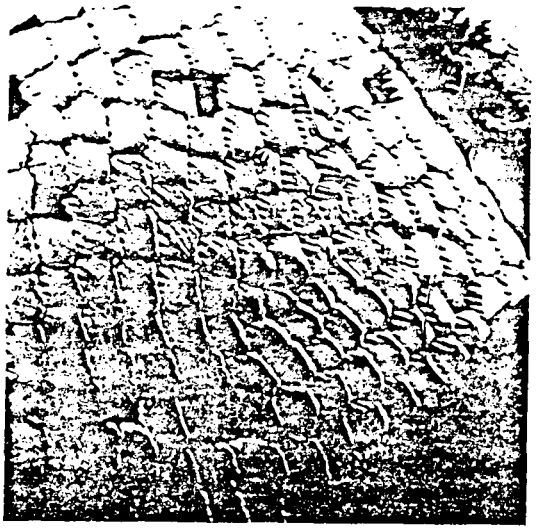

Fig. 2/4: Skin in Tail Region of Black Nose Shark, near the Stagnation Edge (Adult, 1.37 m long, 12x enlargement)

——→ Direction of flow

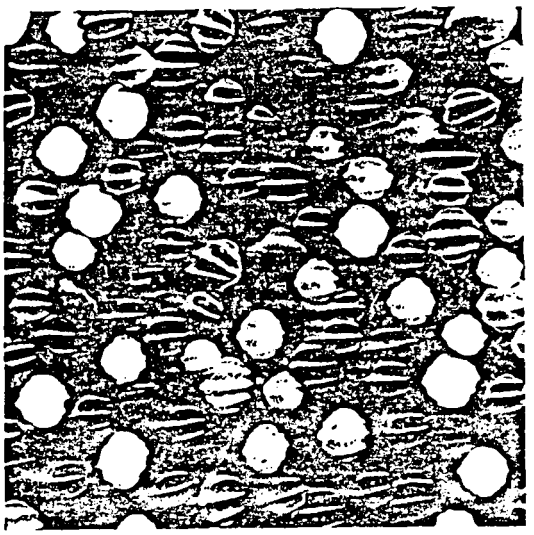

Fig. 2/5: Grooves Scales of an Embryo (Velvet Shark, 0.37 m long, 30x enlargement)

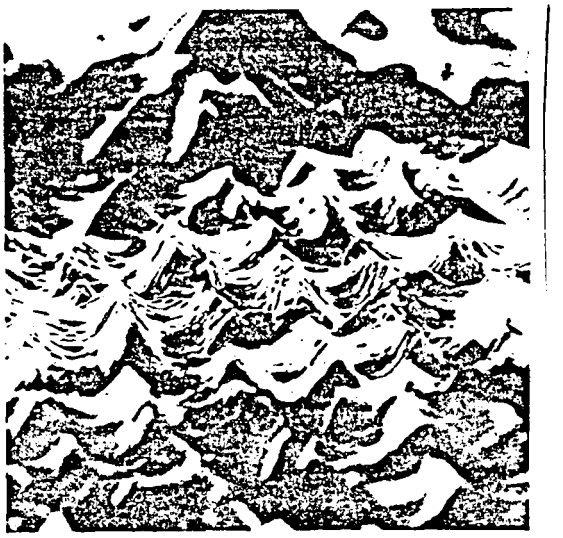

Fig. 2/6: Groove Profile of a Blue Shark (Adult, 2.34 m long, 130x enlargement)

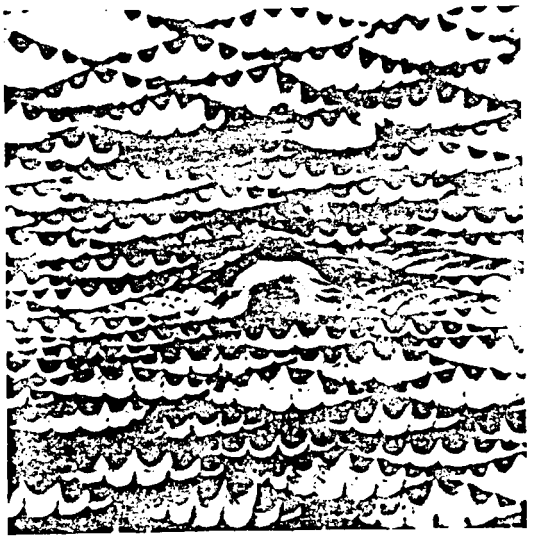

Fig. 2/7: Groove Profile of a Velvet Shark, Viewed from Tail to Head (Adult, 2.30 m long, 64x enlargement)

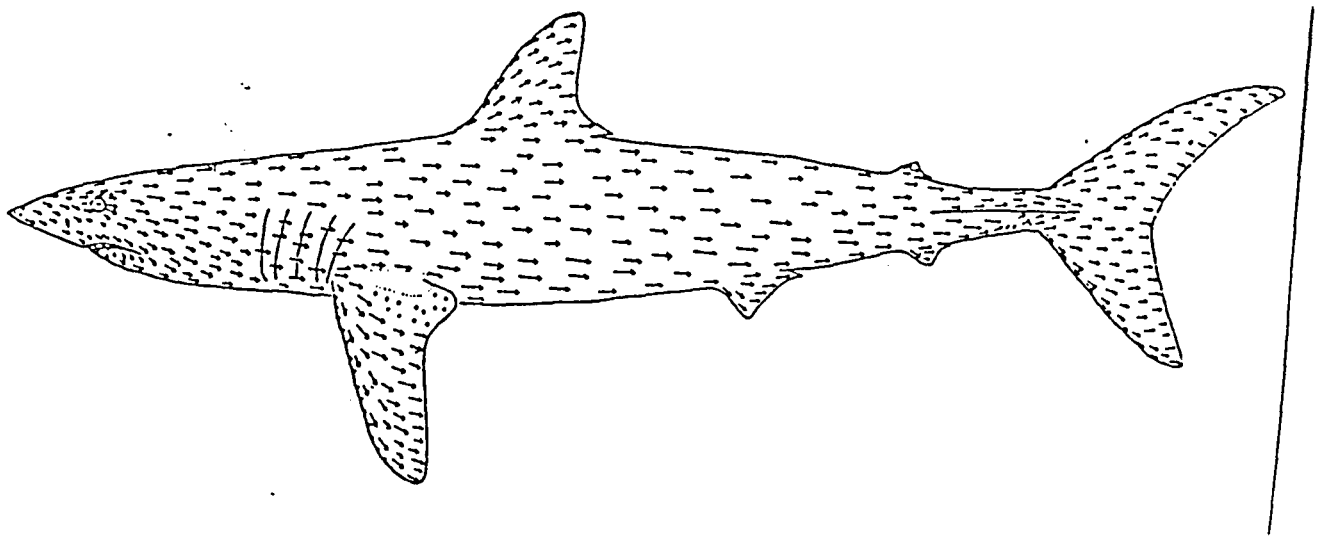

Fig. 2/8: Groove Pattern on a Shark Indicated by Arrows, Dotted Surfaces: Flat scales without grooves (from Reif, Dinkelacker, 1981).

u_∞ m/s		5	10	20
u_τ m/s		0,20	0,40	0,80
1 mit b = 40 µm	b^+	8	16	32
	h^+	3-4	5-8	11-16
1 mit b = 60 µm	b^+	12	24	48
	h^+	4-6	8-12	16-24
1 mit b = 105 µm	b^+	21	42	84
	h^+	7-10	14-21	28-42

Table 2/1: Diminsionless Groove Width b^+ and Groove Height h^+ of the Shark for Various Groove Sizes and Three Flow Velocities u_∞

Key: 1-with

Since the dimensionless groove height h^+ is greater than 5 in the majority of the regions, this roughness should increase the flow resistance of the shark. It is assumed however, that it is just these fast-swimming sharks which are equipped with grooves and that the flow resistance is not increased, at least that flat scales are possible (stagnation edge!). Several other considerations also support the theory of resistance reduction due to the grooves.

2.3 Model conceptions on the Influence of Grooves on Longitudinal Structures in Near-Wall Turbulant Flow

A comparison with the roughness discussed in section 2.1 shows that the grooves offer much less shape resistance since no additional stagnation pressure can occur due to the continuous, longitudinal structure of the grooves. Thus any influence will act primarily via additional, viscous friction.

In figure 2/9 there are some thoughts of Dinkelacker (personal report) in graphic form. The peaks of the groove hills on the shark scales for $h^+ < 24$ are still in a range of the boundary layer in which the viscous portion of the shear stress amounts to about 20% of the total shear stress. A severe change in the viscous portion will thus also be reflected on the total shear stress. If one assumes that the grooves at great distance from the wall have no influence on the velocity profile, then the same velocity will prevail over groove hill and valley. Now since the distance y_B to the groove crest is smaller than y_T to the groove valley, the viscous portion of the shear stress over the groove crest τ_B is greater than that over the groove valley τ_T. In this manner, a strip-structure of τ_w is produced at the wall with a spacing of groove crests which must necessarily have an influence on the near-wall turbulence structure.

According to more recent investigations by Kline et al. (1967) it is just these pronounced longitudinal structures in the immediate vicinity of the wall ($y^+ = 10 - 30$) which have a significant influence on the turbulence generation. In agreement with other authors (Laufer 1975, Willmarth 1975, Blackwelder and Eckelmann 1979, Langeheineken 1981, Kreplin 1976) there exist near the wall, pronounced longitudinal structures, strips of large and small velocity, which have a width of $z^+ \approx 100$.

These results suggest the hypothesis that the grooves on the shark scales cause strips of flow having large and small velocity of groove width $b^+ = 12 - 48$. These smaller structures could reduce the pulse exchange and thus also the energy dissipation.

Similar considerations and initial measurements have also been made by Hefner, Weinstein, Bushnell (1980) and Walsh (1980). Hefner, Weinstein and Bushnell see two possibilities for influencing the turbulent motion. "Evidently there are two possibilities for getting at this problem (namely, control of turbulence): 1) Introduction of

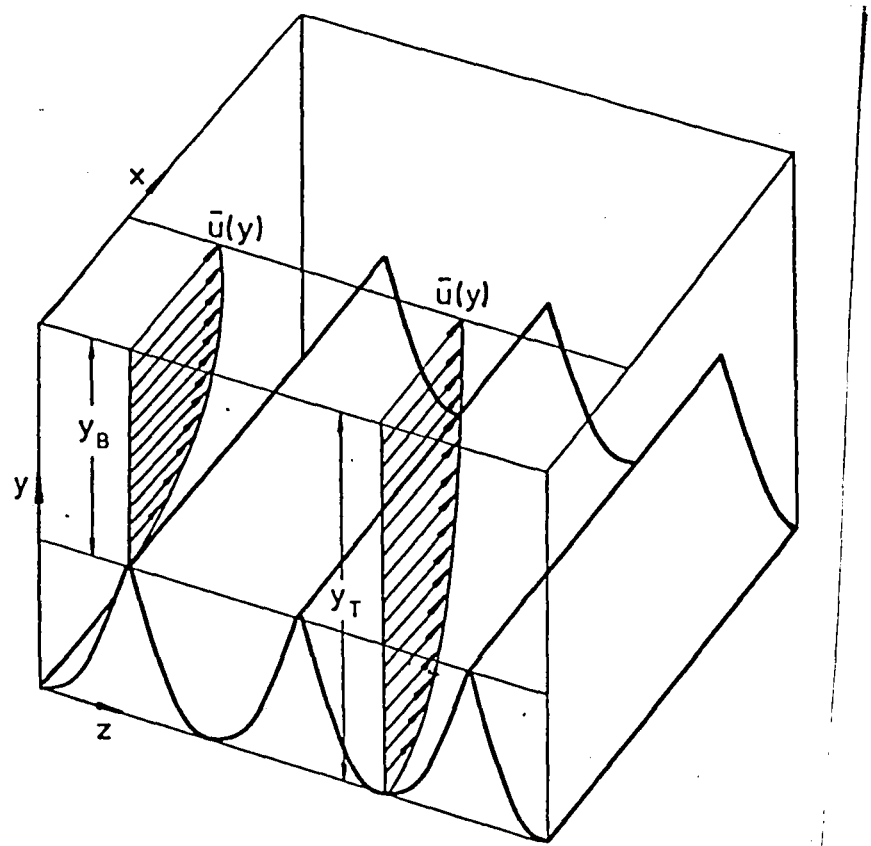

Fig. 2/9: Schematic Illustration of Model Conception of the Influence of Grooves on near-wall turbulent Flow (from Dinkelacker, personal report).

interference bodies into the farther-out boundary layer flow in order to destroy large structures, or 2) The use of uneven walls in order to exert via the wall geometry an influence on near-wall strips of small and large velocity and/or the burst phenomenon." But they are concerned with the first possibility, whereas the work by Walsh, like the present paper, is concerned with the second possibility. Walsh used a plate with V-shaped, longitudinal grooves with dimensionless groove spacing $b^+ = b \cdot \frac{u_\tau}{\nu} < 200$ and groove height $h^+ = h \cdot \frac{u_\tau}{\nu} < 25$ and found a maximum reduction in resistance of 7% compared to the smooth plate.

3. Test Set-up

3.1 Tube Channel

To perform the investigations, an open tube channel system was set up (fig. 3/1). It was powered by a three-phase-driven radial fan whose RPM is continuously controlled by a frequency converter. Flows of 3.5 l/s to 50 l/s can be attained; with the outlet-connected throttle valve, the flow can be cut down to 2 l/s. Behind the valve

there is an installed sound damper in which the air is fed through ca. 3 m-long; bent and rockwool-lined channels in order to dampen the noise of the fan. The air moves through a large-diameter hose into the spin flow meter (Fischer & Porter Model D 10 SG 4211 AEEE). A short connector tube carries it to a thermometer in the contact zone with the prechamber which contains an air filter and rectifier. The air moves through an edged inlet into the mounted tube. Since the tubes are of different diameter, a corresponding connector flange was prepared for each tube; this permits a smooth transition (fig. 3/2). On the free end of the tube a flange is set on (fig. 3/3) and it serves to attach the sliding device. With this sliding device a hot-wire probe or Pitot tube can be moved precisely perpendicular at 1/10 mm accuracy (for adjusting to tube middle) and horizontally to 1/100 mm (for adjusting the wall distance y when measuring the profile) over the tube cross-section. The tubes lie on two Dexion rails and are elastically suspended with the support lane to insulate against sound transmitted through solids.

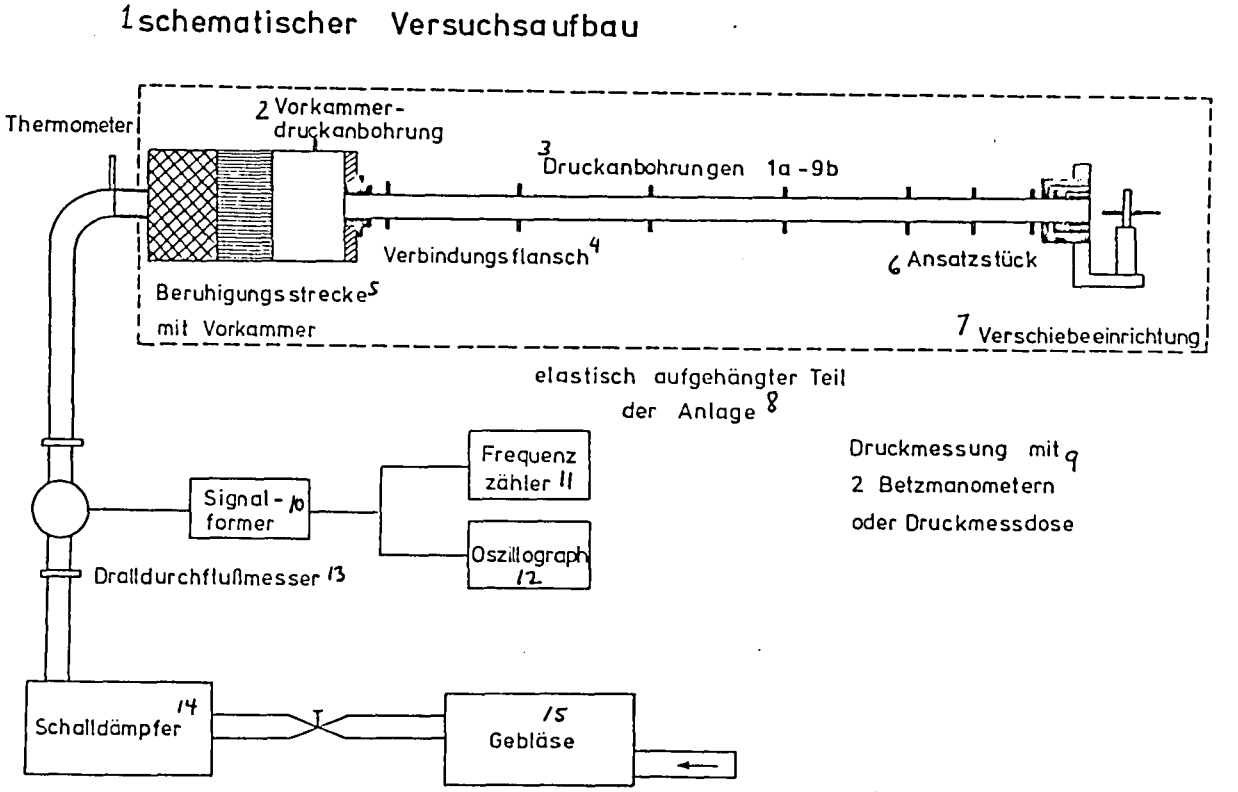

Fig. 3/1: Schematic Test Set-up of the Tube Channel System

Key: 1-schematic test set-up 2-prechamber pressure hole 3-pressure holes 4-connecting flange 5-support lane 6-set-on piece 7-sliding device 8-elastically suspended part of the system 9-pressure measurement with two Betz manometers or pressure measuring cans 10-signal shaper 11-frequency counter 12-oscilloscope 13-spin flow meter 14-noise damper 15-fan

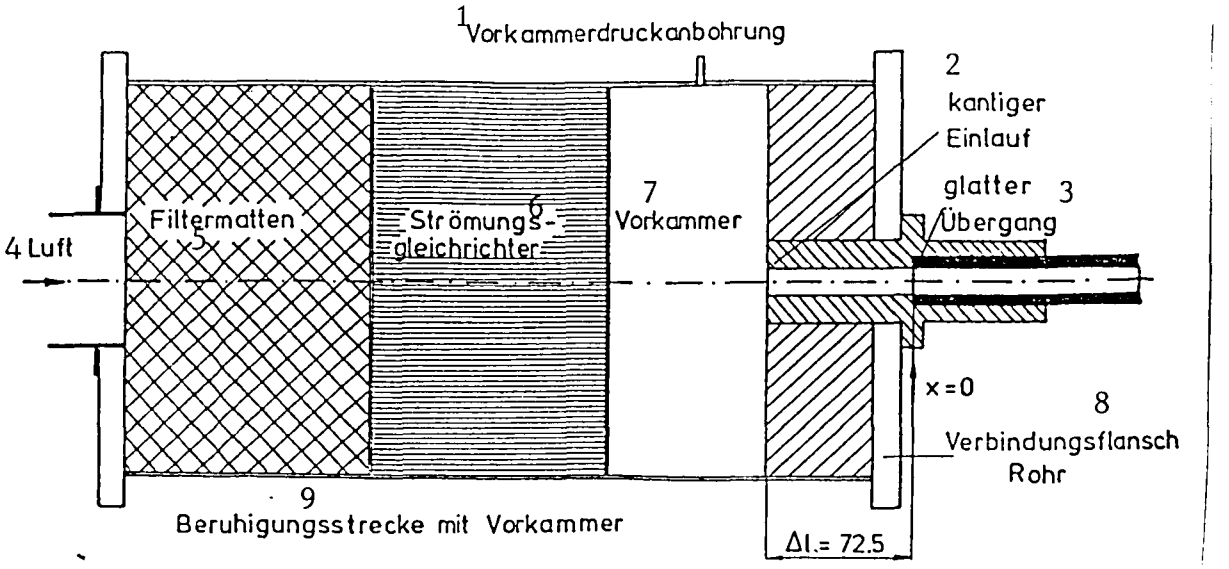

Fig. 3/2: Calming Lane with Prechamber and Connector Flange for Smooth Transition into the Particular Tube

Key: 1-prechamber pressure hole 2-edged inlet 3-smooth transition 4-air 5-filter mat 6-flow rectifier 7-prechamber 8-connecting tube flange 9-calming lane with prechamber

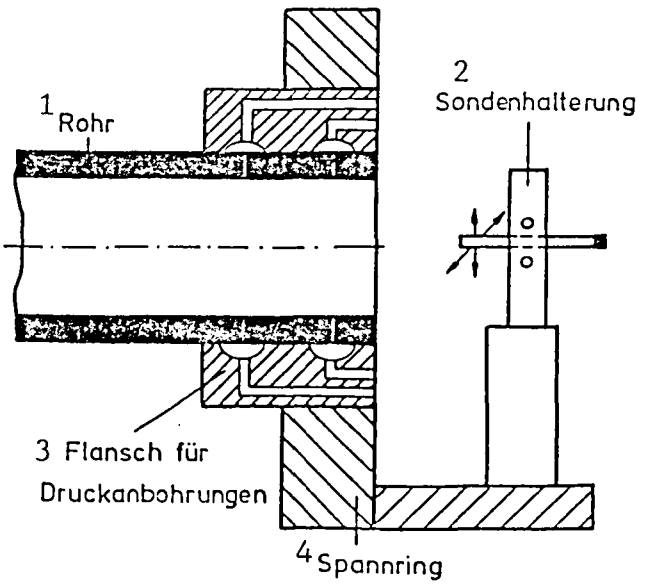

Fig. 3/3: Flange with Pressure Holes for Attachment of the Sliding Device

Key: 1-tube 2-probe mount 3-flange for pressure holes 4-tension ring

3.2 Tubes

The following four tubes were used for the measurement:

Rohr Nr.	Material	Länge [m]	Art	Durchmesser d bzw. d_I^* [mm]	Fehler des Mittelwertes [mm]	maximale Abweichung [mm]
R 1	Aluminium	5,00	glatt	39,89	$\pm$ 0,00	0,01
R 2	PVC	4,93	glatt	42,31	$\pm$ 0,02	0,12
R 103	PVC	5,00	Rillen	38,20 *	$\pm$ 0,01	0,13
R 105	PVC	5,00	Rillen	42,13 *	$\pm$ 0,01	0,05

Table 3/1: Technical Details on the Used Tubes.

*d_I is the diameter of a circle touching the peaks of the groove crests.

Key: 1-tube no. 2-material 3-length 4-type 5-diameter d or d_I 6-error of average value 7-maximum deviation 8-aluminum 9-smooth 10-grooves

The diameters were measured with a tripod inside micrometer with an accuracy of 0.005 mm. About 20 measurements at different locations inside the tube and under different angles were taken for averaging. Besides the average values, the error of the average (for tube R1 this error is less than 0.005 mm) and the maximum deviation from the average are provided.

The grooved tubes were produced by Hoechst AG, Frankfurt, with 240 grooves at a groove spacing of about 0.5 mm. With this groove spacing we can cover the range of average velocity u_M of 3 m/s to 40 m/s in the range of $b^+ = b \cdot \frac{u_\tau}{\nu}$:

u_M [m/s]	3	40
u_τ [m/s]	0,12	1,60
b^+	3,9	52

Table 3/2: Attainable Values for Dimensionless Groove Width b^+ on Grooved Tubes at the Average Velocity Specified by the Test Set-up

The microscopic photos (fig. 3/4) show the groove shape of tube R 103 and R 102 (cross-section) with a scale. For technical reasons, the groove shape could not be better adapted to the grooves on the shark scale. A microscopic measurement taken with the conditions of fig. 3/5 showed:

	R 103	R 105
h [mm]	0,13	0,50
b [mm]	0,50	0,55
$\frac{h}{b}$	0,26	0,91
A $[mm]^2$	0,046	0,117

Table 3/3: Dimensions of the Groove Structure, Size Designations from Figure 3/5.

The cross-sectional area between all 240 grooves (240 A) amounts to 1.0% for tube R 103, and to 2.0% for tube R 105, of the total cross-sectional area.

Since the friction also increases with increasing surface area, the surface enlargement shall be given here as a ratio of the surface in a tube of the same diameter. For tube R 103, this amounts to about 50% and for tube R 105, to about 100%.

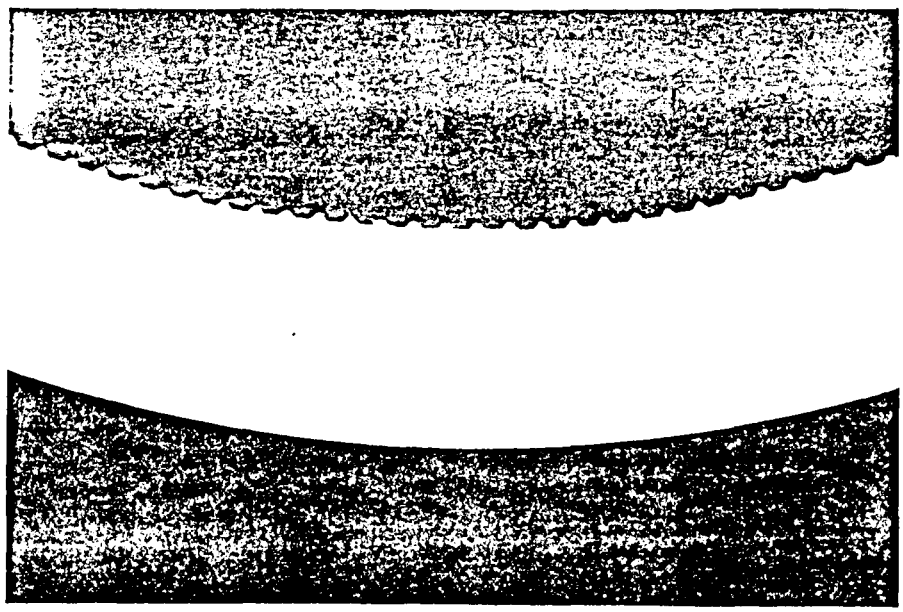

Fig 3/4(a): Groove Profile of the Two Grooved Tubes.
(a) Tube R 103

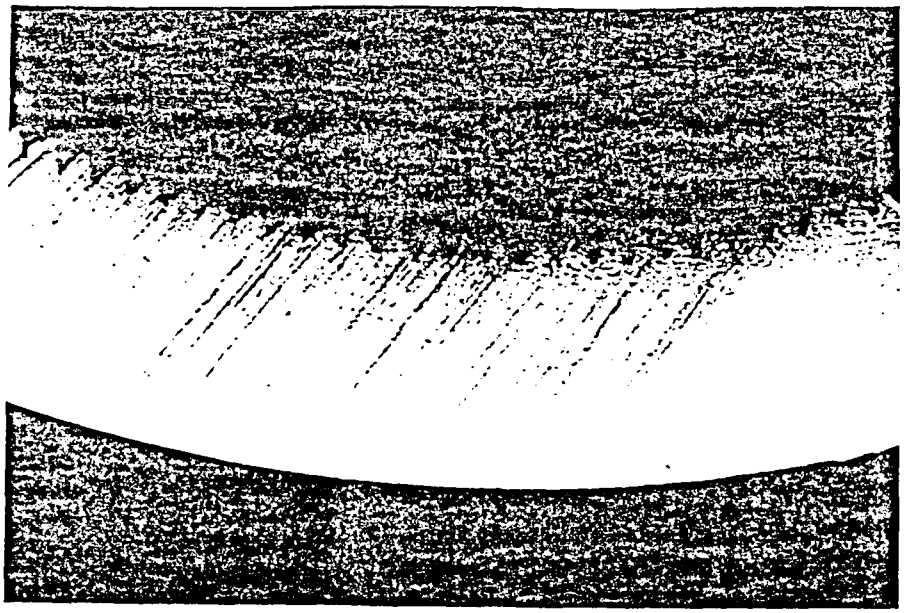

Fig. 3/4(b): Groove Profile of the Two Grooved Tubes.
(b) Tube R 105

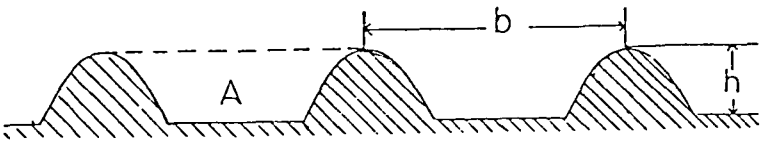

Fig. 3/5: Cross-Sectional View of the Grooved Tubes

3.3 Pressure Holes

Tubes R1, R103, R105 are equipped with 18 pressure holes of 1 mm diameter; tube R2 has 12 such holes, all arranged in pairs. They are located at the following distances from the beginning of the tube (x = 0):

x[m]	Nr. der Anbohrung bei Rohr 1	
	R 1, R 103, R 105	R 2
0,05	1A, 1B	1A, 1B
1,03	2A, 2B	2A, 2B
2,01	3A, 3B	3A, 3B
2,99	4A, 4B	4A, 4B
3,97	5A, 5B	5A, 5B
4,46	6A, 6B	- -
4,87	- -	7A, 7B
4,95	7A, 7B	- -
4,975	8A, 8B	- -
4,99	9A, 9B	- -

Table 3/4: Position x and Number of Pressure Holes on the Four Tubes
Key: 1-no. of drilled hole for tube

To remove the drilling burrs, a counterpiece was run through the tube after drilling; for the grooved tubes a casting of the grooves was produced. Hose lips of 2 mm diameter are attached to drilled holes 1a to 7b. Holes 8a to 9b go out beyond the edge via the flange and are provided with hose lips there (fig. 3/3). The set-on pressure hoses run through two distributors to two Betz manometers.

The pressure drop was measured via pressure holes by using a Betz manometer. A more accurate description of the measurement method and discussion of measurement accuracy are provided in section 4.2.

3.4 Electronic Section

To measure the average velocity $\bar{u}$ and the velocity fluctuations u', the circuitry shown in figure 3/6 was set up.

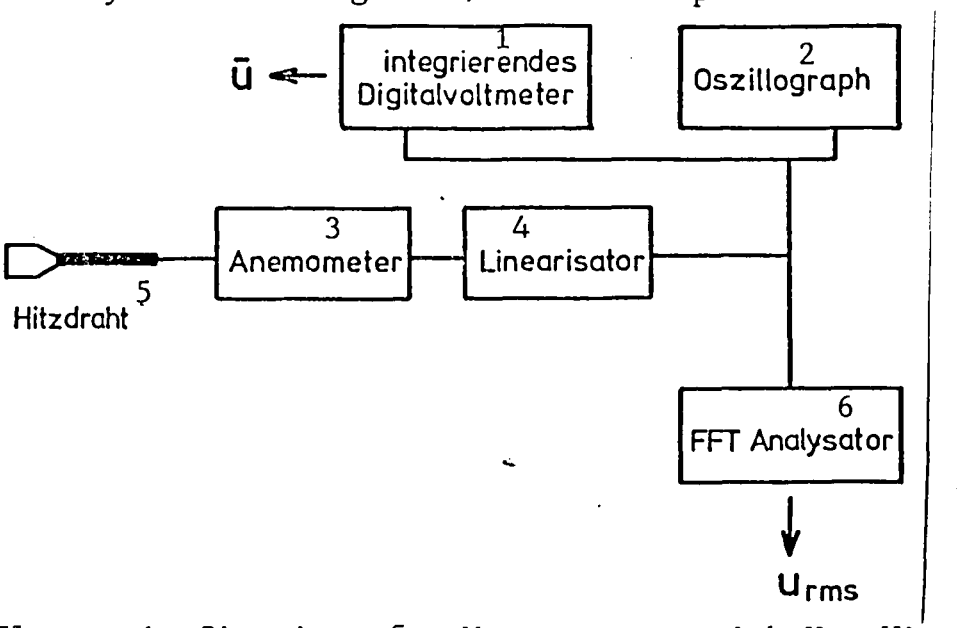

Fig. 3/6: Electronic Circuitry for Measurements with Hot-Wire Probe

Key: 1-integrated digital voltmeter 2-oscilloscope 3-anemometer 4-linearizer 5-hot wire 6-FFT analyzer

The used instruments are described in table 3/5.

Anemometer, Disa type 55 M01
Linearizer, Disa type 55 D10
Integrated digital voltmeter, Hewlett Packard 5335 A
Oscilloscope, Philipps PM 3234
FFT Analyzer, Nicolet Scientific Corp. 660A

Table 3/5: List of Used Electronic Instruments

Measurement methods and error discussion are presented in section 5.2.

4. Flow Resistance of the Investigated Tubes

4.1 General Fundamentals on the Resistance Law

Friction losses in a turbulent tube flow with smooth walls were produced by various mechanisms. Through the dynamic viscosity μ of the medium, there result between layers of different velocity, stresses which cause friction loss. These stresses are of great significance near the wall ($y^+ < 7$), since turbulent motion there is small, but the velocity gradient is large. For larger wall distances $y^+ > 50$ (Rotta, 1972, p. 155) the losses due to turbulent motion of the medium will predominate. This motion causes an additional pulse exchange between the layers of different, average velocity $\bar{u}$ of the flow and thus additional stresses $\tau = -\varrho \overline{u'v'}$. In the rough tube, the effect of both mechanisms is increased. The enlarged surface causes an additional, viscous friction. The shape resistance of the individual roughness elements produces pressure losses which converts energy into additional turbulent motion (Rotta 1972, p. 159, Prandtl 1969, p. 191).

After the inlet length of about 50 diameters (see section 4.2.2) the velocity profile typical for turbulent tube flow and the particular Reynolds number is formed. Now since on average no accelerations occur, the pressure and friction forces must be in equilibrium. Since all friction effects act on the wall, they can be summarized in the wall shear stress τ_w. Thus, for the force equilibrium at a pressure drop Δp over distance l, we have:

$$\tau_w \pi \cdot d \cdot l = \Delta p \cdot \pi \frac{d^2}{4}$$

$$\tau_w = \frac{\Delta p}{l} \cdot \frac{d}{4} .$$

The friction losses can thus be described by $\frac{\Delta p}{l}$. In order to have a dimensionless representation of a resistance law for tubes, the dimensionless resistance factor is defined as:

$$\lambda := \frac{\frac{\Delta p}{l} \cdot d}{\frac{\varrho}{2} u_Q^2} , \qquad (4.1)$$

(u_Q: Average velocity)

which corresponds to the ratio of wall shear stress and average kinetic energy per volume (except for a number factor):

$$\lambda \sim \frac{\text{Wall shear stress}}{\text{Kinetic energy per volume}}$$

λ can be a function of the density ϱ, viscosity μ, average velocity u_Q and of the tube diameter d.

$$\lambda = f(\varrho, \mu, u_Q, d)$$

The single most simple and dimensionless combination of these quantities is provided by the Reynolds number:

$$Re = \frac{u_Q \cdot d}{\frac{\mu}{\varrho}} = \frac{u_Q \cdot d}{\nu} \qquad (4.2)$$

Therefore it is expected that λ is only a fraction of the Reynolds number (Becker 1974, p. 102f).

$$\lambda = f(Re) = f\left(\frac{u_Q \cdot d}{\frac{\mu}{\varrho}}\right)$$

This dependence is called the resistance law.

For a laminar flow, λ can be calculated according to the Hagen-Poiseuille theory:

$$\lambda = \frac{Re}{64}$$

For a turbulent flow, Blasius formed the Blasius law from numerous measurements (Schlichting 1965, p. 554, Blasius 1913):

$$\lambda = 0{,}3164\ Re^{-0{,}25} \qquad (4.3)$$

Figure 4/1a shows results of various measurements taken from Schlichting (1965, p. 554). In addition, figure 4/1b illustrates the measurements mentioned in section 2.1 on sand-rough tubes made by Nikuradse (Schlichting 1965, p. 572).

For future consideration, additional variants shall be given. With:

$$u_\tau := \sqrt{\frac{\tau_w}{\varrho}} = \sqrt{\frac{\frac{\Delta p}{l} \cdot \frac{r}{2}}{\varrho}} \qquad (4.4)$$

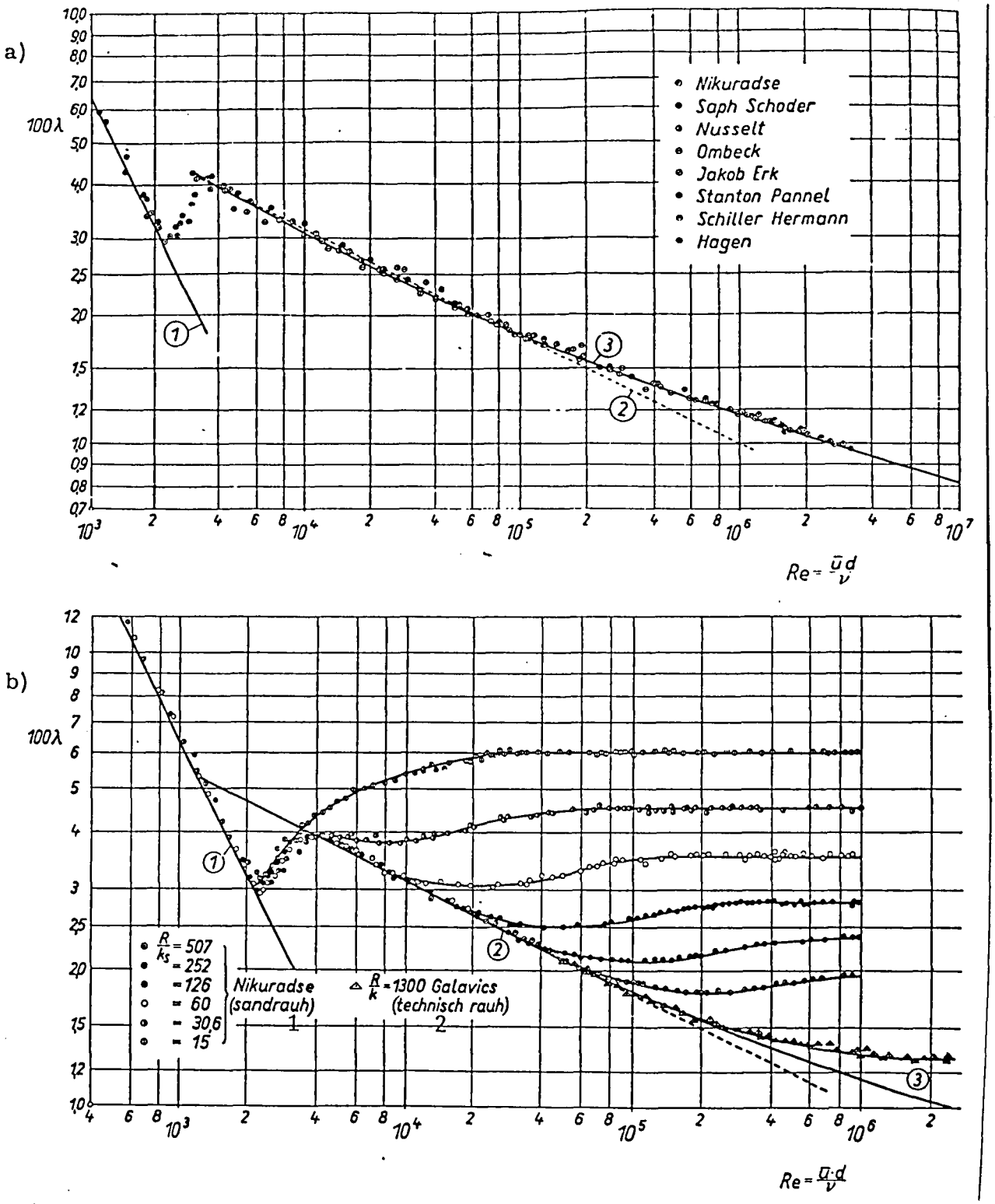

Fig. 4/1: a) Resistance Law of Smooth Tube, Values from Various Authors
b) Resistance Law for Rough Tubes, Values from Nikuradse
1) $\lambda = Re/64$ from Hagen Poiseuille
2) $\lambda = 0.3164 \cdot Re^{-0.25}$ from Blasius
3) $1/\lambda = 2.0 \log (Re\sqrt{\lambda}) - 0.8$ from Prandtl
(Schlichting 1965; a) p. 554; b) p. 572

Key: 1-sand-rough 2-technical rough

there follows from (4.1):

$$\lambda = 8 \cdot \left(\frac{u_\tau}{u_Q}\right)^2 \qquad (4.5)$$

Since the flow-through Q was measured directly in this paper, (4.1) and (4.2) shall be converted into:

$$\lambda = \frac{\frac{\Delta p}{l} d^5}{Q^2 \cdot \varrho} \cdot \frac{\pi^2}{8} \qquad (4.6)$$

and

$$Re = \frac{Q}{d\nu} \cdot \frac{4}{\pi} \qquad (4.7)$$

To compute the resistance law from eq. (4.6) and (4.7), the following 5 quantities must be measured:

Flow-through Q
Pressure drop $\frac{\Delta p}{l}$
Tube diameter d
Density ϱ
Dynamic viscosity μ

The measurement methods and their accuracy shall be described below.

4.2 Measurement Methods and Accuracy

4.2.1 Measurement of the Flow-Through

The flow-through was measured with the spin flow meter (DDM). An eddy current is produced in the inlet of the DDM; this eddy becomes instationary in a short diffusor. In this manner, a secondary rotation of the eddy core results whose frequency is approximately proportional to the flow-through. The temperature-sensitive resistor heated and installed in the diffusor, picks up the rhythmic cooling due to the eddy core. The oscillation is amplified and converted into a rectangular pulse, so that the frequency can be measured very simply with a counter. The flow can be read off a manufacturer-delivered calibration curve as a function of the frequency to within 0.25% accuracy. Errors due to losses or leaks are prevented by a careful sealing. It was checked by sealing off the system in front of the DDM and at the tube end and adding compressed air. It turned out that the loss for all flows was less than 0.01%. In order to prevent rough deviations in the specification of the spin

flow meter, one profile was measured for 3 Reynolds numbers ($Re \cdot 10^{-4}$ = = 1.0...2.3...3.4) with the hot-wire probe and a deviation of 1.8%, 1.1% or 0.5% was found. Since the hot-wire probe itself measures only to 2% accuracy, there is good agreement and the accuracy statement of the manufacturer can be used. Systematic errors in the DDM will have only an influence on a comparison of results from the smooth tube with results of other authors. A comparison between grooved tubes and smooth tubes would not be affected by a systematic error.

Since the DDM measures the volume of the compressed, flowing gas, for greater pressures in the DDM, a conversion to outside pressure is needed:

$$Q = Q_{measured} \cdot (1 + \frac{p_{DDM}}{p_o})$$

The flow-through could thus be measured over a wide range (4 - 56 l/s) to an accuracy of 0.25%.

4.2.2 Determination and Accuracy of the Average Pressure Drop

a) Measurement Principle

Initially, all pressures p_i were measured and recorded at the drill holes 1A to 9B. Figures 4/2 to 4/5 show these pressures as a function of the tube longitudinal coordinate x at the four tubes for 4 different flows each. The results from a- and b-holes are entered separately; a comparison of pressure values from opposing holes is presented farther below.

To compute the pressure drop, the inlet requires particular attention since in the tube inlet, no equilibrium has been established between the friction forces and pressure forces; the average velocity $\bar{u}$ is still dependent on the run-length x and the wall separation y. For the formation of the velocity profile typical for the particular Reynolds number, additional kinetic energy is needed so that for smaller values x, a greater pressure drop is expected. Since the inlet is angular in the used test set-up, strong turbulent exchange motions will result, even at small x-values so one can expect a relatively short inlet length. According to measurements by Kirsten (1927), the inlet length is 50 to 100 tube diameters; Nikuradses (1932) measurements showed a well-formed profile after only 25 to 40 tube diameters. In several figures 4/2 to 4/5 one can see (for larger flows Q), that p_1 and p_2 lie above the lines p(x). The additional loss of kinetic energy shows up in these measurements within a length of x = 2m or about 50 tube diameters. Thus, the results presented here lie within the measured range of other experimentors. To compute the pressure drop in the course of the well-formed part of the flow, a compensation line is drawn using the method of smallest error quadrants and running through the points p_3(x=2.01 m) to p_9(x = 4.99 m).

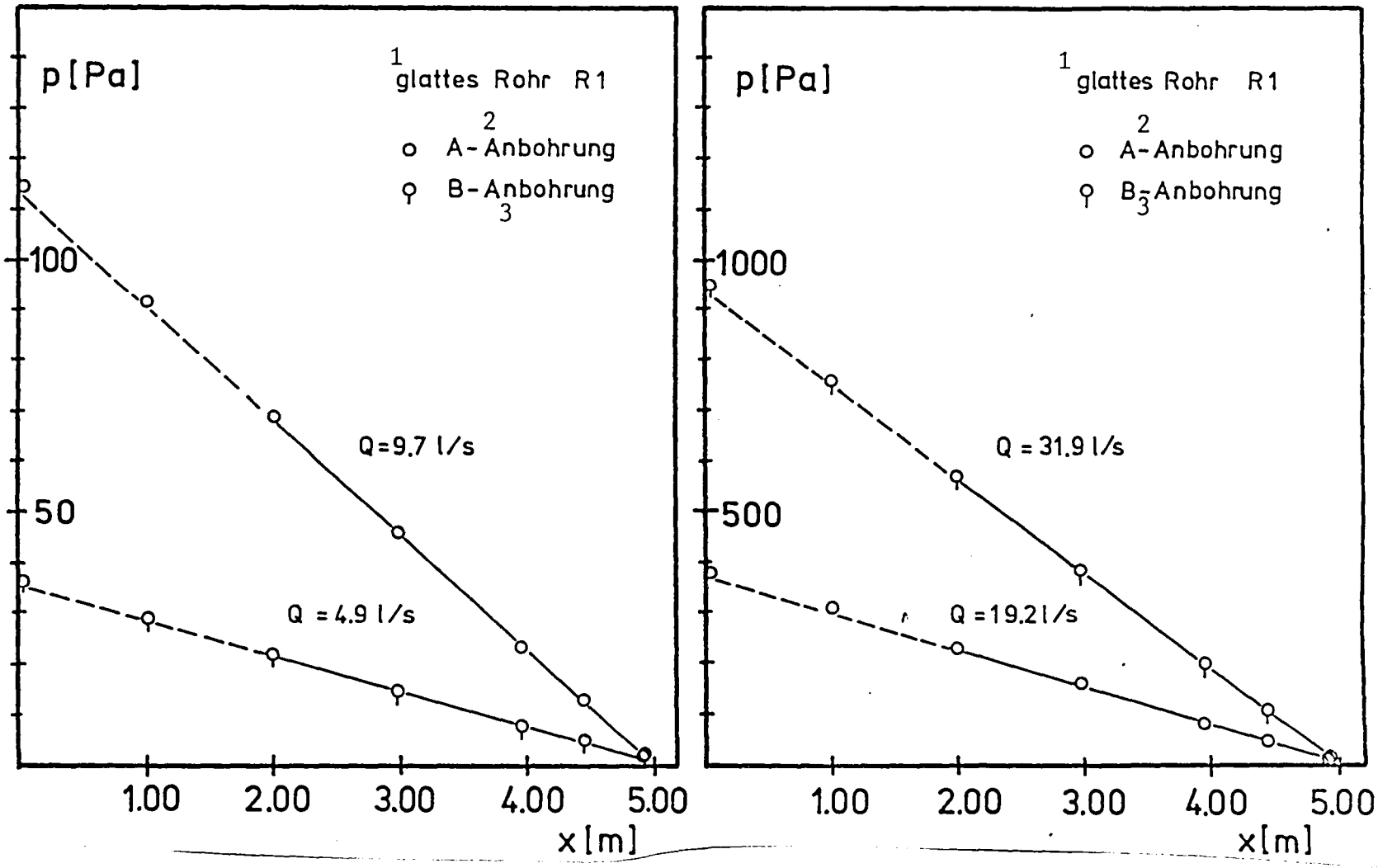

Figure 4/2: Pressure Drops p = p(x) for a Smooth Tube R1 at Different Flows

Key: 1-smooth tube 2-A-hole 3-B-hole

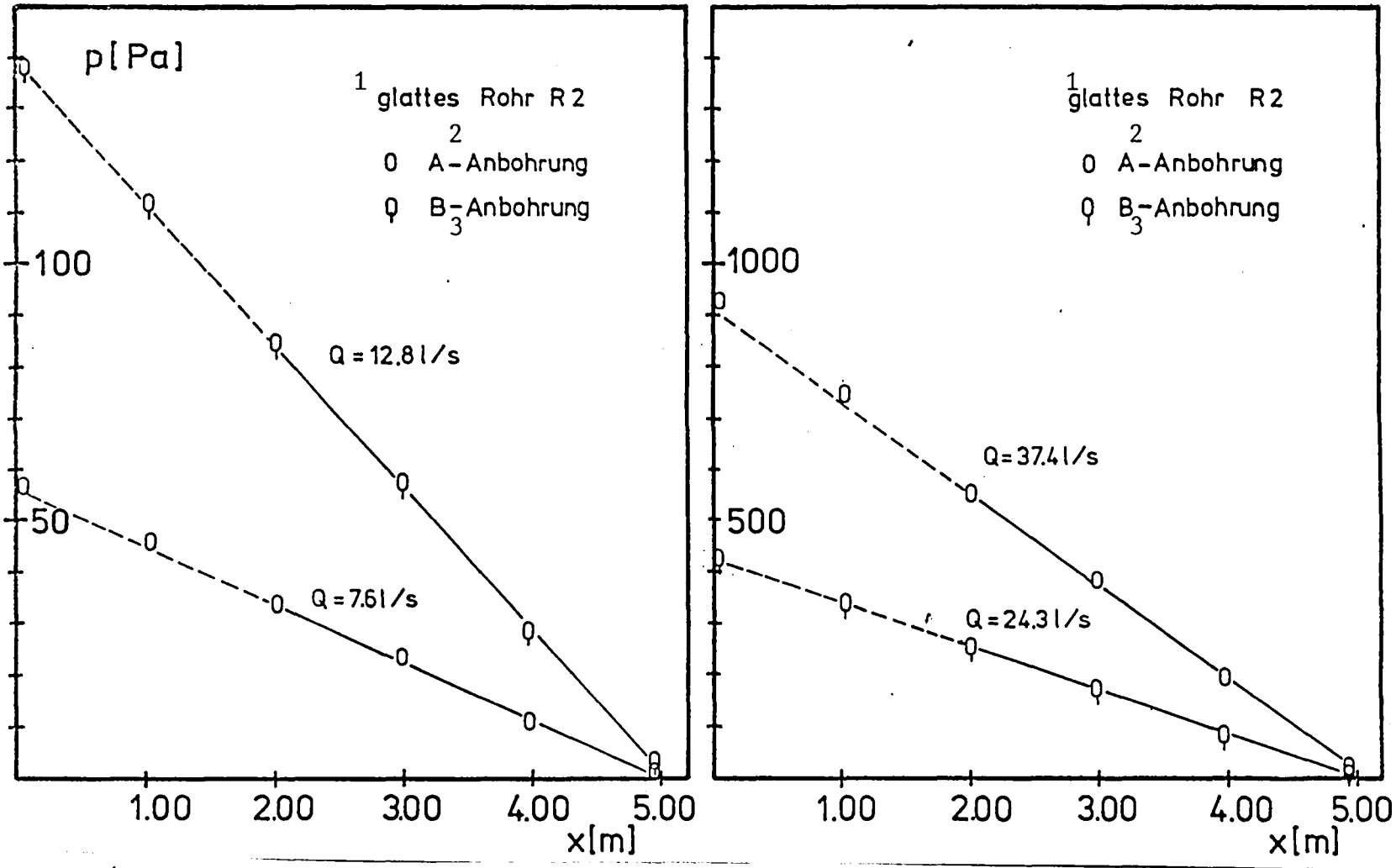

Fig. 4/3: Pressure Drops p = p(x) for a Smooth Tube R 2 at Different Flows

Key: 1-smooth tube 2-A-hole 3-B-hole

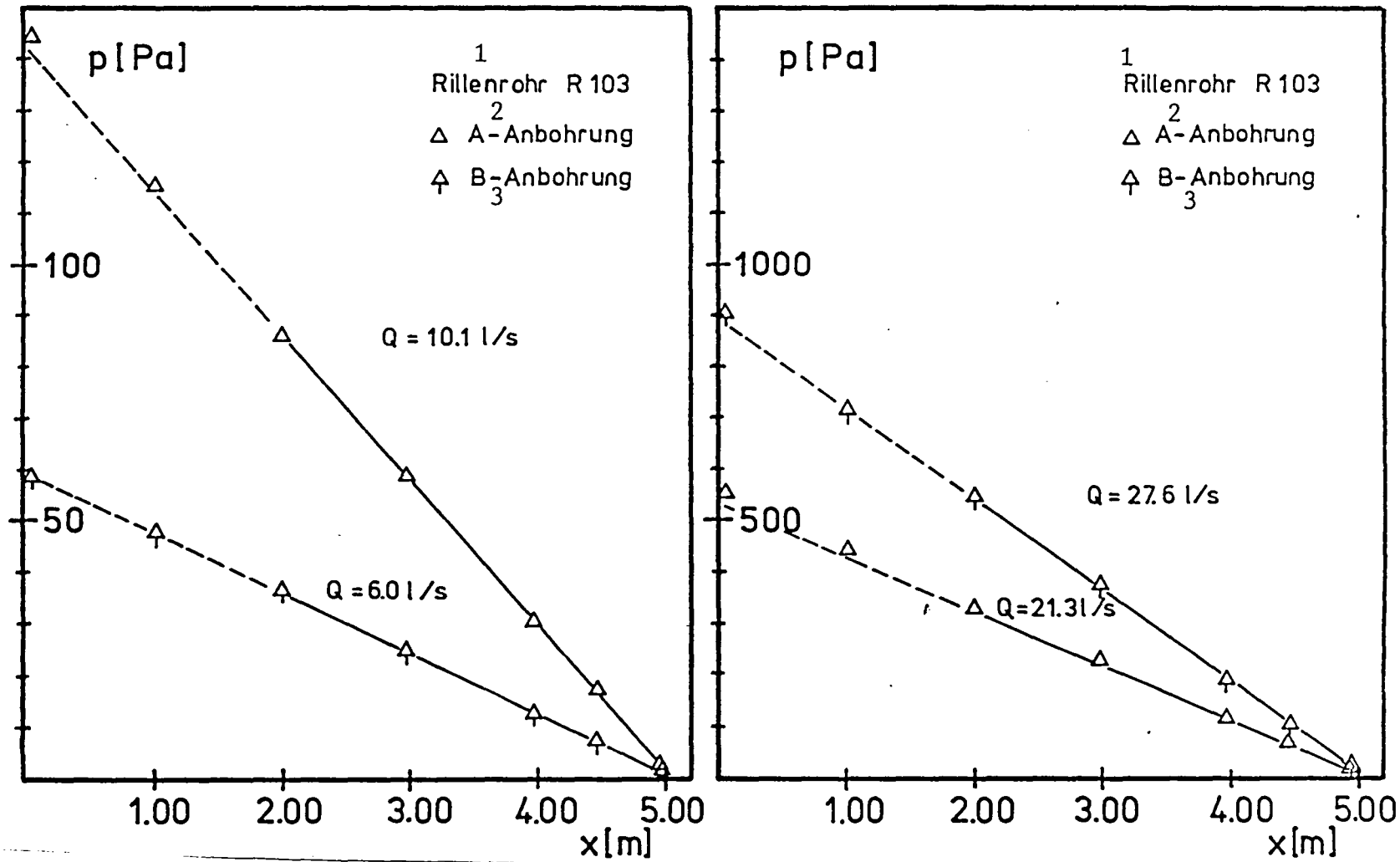

Fig. 4/4: Pressure Drops p = p(x) on a Grooved Tube R 103 for Different Flows
Key: 1-grooved tube 2-A-hole 3-B-hole

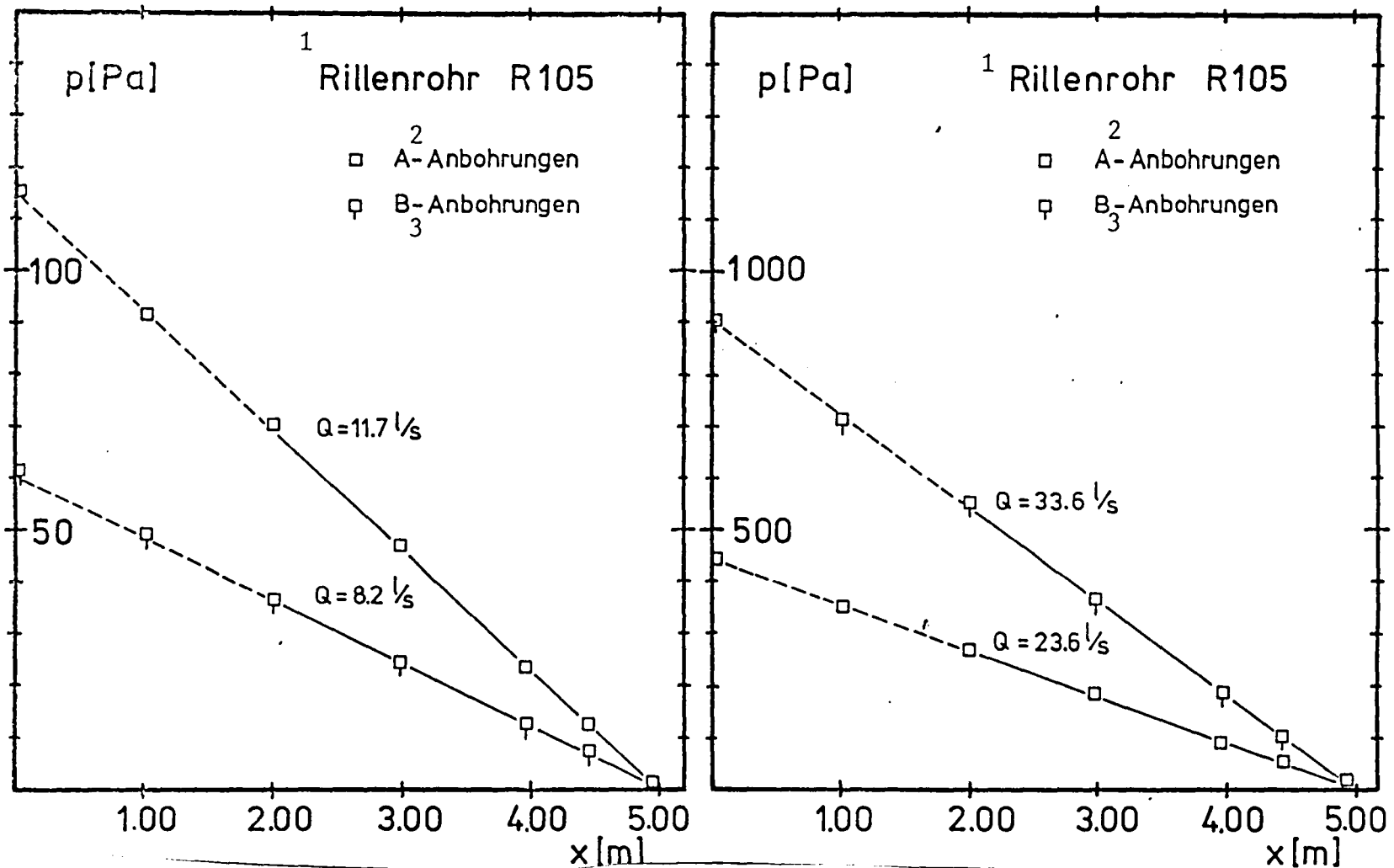

Fig. 4/5: Pressure Drops p = p(x) on a Grooved Tube R 103 for Different Flows
Key: 1-grooved tube 2-A-holes 3-B-holes

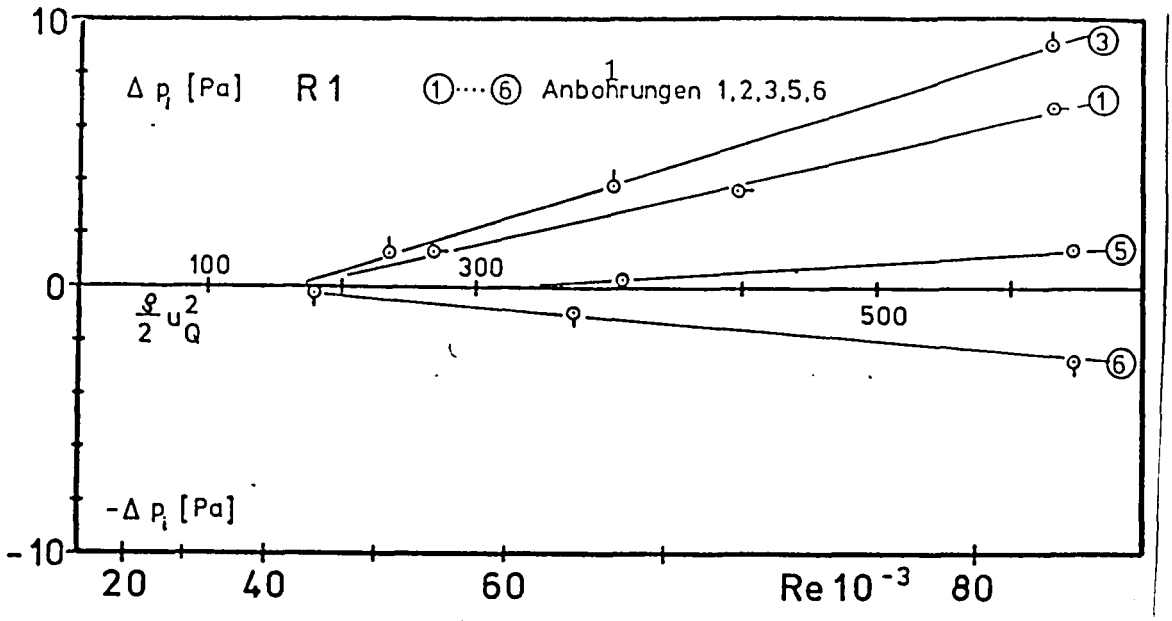

Fig. 4/6: Pressure Differences $p_i = p_{iA} - p_{iB}$ Between Two Holes i at the Same Position x on a Smooth Tube R1 as a Function of the Average Stagnation Pressure $\frac{\varrho}{2} u_Q^2$.

Key: 1-drill holes

In an estimation of the accuracy of the pressure drop, two questions arise: How accurate are the pressure measurements of the individual drill hole? How do errors in a drill hole affect the determination of the average pressure drop?

b) Accuracy of Pressure Measurement, Especially for Grooved Tubes

Pressure measurements through drill holes in grooved tubes require special attention since from numerous investigations (e.g. Franklin and Wallace 1970) it is known that drilling burrs or small interference bodies in the environ of the drill hole, have a severe influence on the measured results. From a paper by Polzin (1939) on pressure holes in sand-rough walls (height of sand roughness about the same magnitude as the groove height h used here) one can find the following results:

-For smooth walls, a careful removal of the drilling burr is of great importance. Measurements of the static pressure deviate in a positive and negative direction from the true pressure.

-Errors in the pressure measurement in drill holes in smooth and rough walls are about the same order of magnitude.

-The difference between measured pressure and true pressure Δp_{st} with respect to the average stagnation pressure $\frac{\Delta p_{st}}{\frac{\varrho}{2} u_Q^2}$ is:

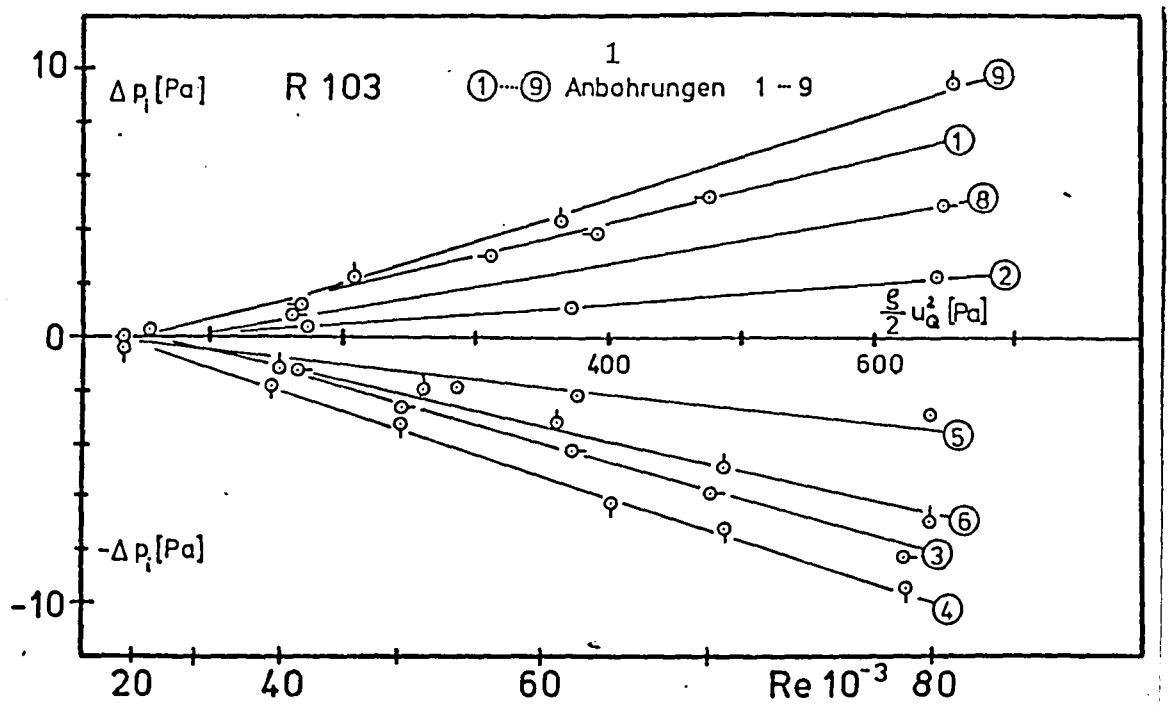

Fig. 4/7: Pressure Differences $p_i = p_{iA} - p_{iB}$ Between Two Drill Holes i at the Same Position x on a Grooved Tube R 103 as a Function of the Average Stagnation Pressure $\frac{\rho}{2} u_Q^2$.

Key: 1-drill hole

- near zero and proportional to the Reynolds number for a preset roughness
- large zero for downstream roughness and independent of the Reynolds number
- indifferent for roughness lying to the side.

In order to check the accuracy of our pressure measurements, the pressure differences $\Delta p_i = p_{iA} - p_{iB}$ between the opposing drill holes i, i = 1...9 were measured; these would have to equal zero for an error-free measurement. They are entered in figures 4/6 to 4/8 as functions of the average stagnation pressure $\frac{\rho}{2} u_Q^2$. For the smooth tube R1, only a few of the largest pressure differences Δp_i are entered. As one can see, the pressure difference increases with increasing groove depth from tube R 103 to R 105; it is smallest for the smooth tube and is more rare. The relationship between Δp_i and $\frac{\rho}{2} u_Q^2$ can be easily represented by a line. Thus, the increase $\frac{\Delta p_i}{\frac{\rho}{2} u_Q^2}$ becomes a relative error and depends on the Reynolds number. With the exception of the strong, relative error on tube R 105 for drill holes 3, 4 and 6, the relative errors are about the same size as those measured by Polzin. Since two potentially incorrect pressure

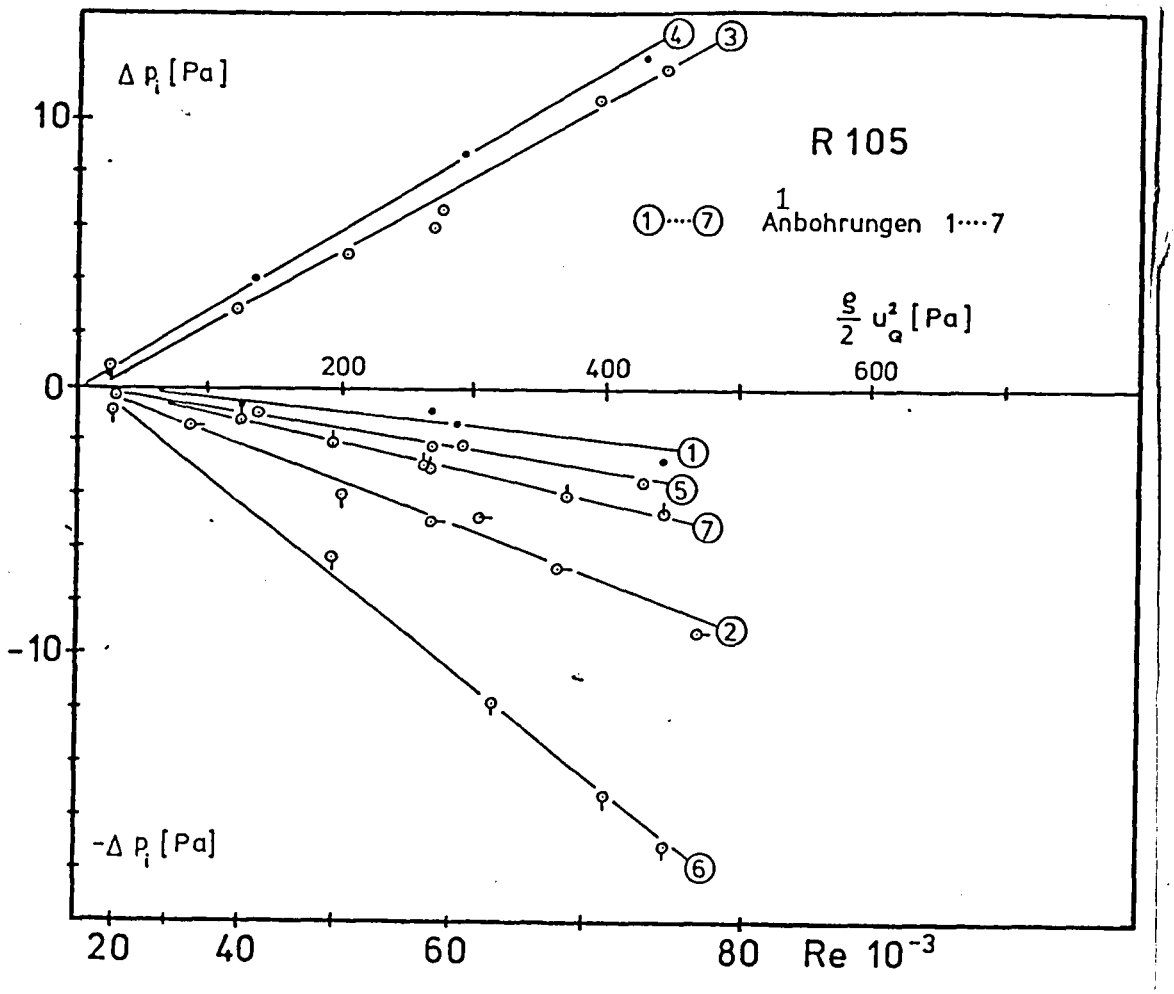

Figure 4/8: Pressure differences $p_i = p_{iA} - p_{iB}$ Between 2 Drill Holes i at the Same Position x on a Grooved Tube R 105 as a Function of the Average Stagnation Pressure $\frac{\rho}{2} u_Q^2$.

Key: 1-drill holes

measurements are being compared here, it is not possible to differentiate between pressure and suction effect by means of roughness and thus to draw conclusions about the direction of the systematic deviation.

As possible correction, one could perform averaging between the pressures at the opposing drill holes. This correction was performed on several pressure profiles p(x). For two reasons however, this correction was not used below: First, the average quadratic deviation of the corrected pressures p to the compensation lines p = p(x) are not smaller over the majority of the pressure profiles and the accuracy is thus not definitely better. Second, the change between corrected and uncorrected pressure drops is negligible (on average 0.4%).

c) Accuracy of the Average Pressure Drops

As in the preceeding section, the errors in the pressure measurement are of a systematic nature for the individual drill holes. But one can assume that for a large number of pressure holes in the grooved tubes, the measured pressure values are normally distributed for the same, true static pressure. The groove crest lying in front of the drill hole cannot be viewed as preset roughness since it is not set in as an elevation in front of the hole, but is extended toward the tube beginning. With preset roughness the dependence on Reynolds number also drops out, which is confirmed by the linear relationship of pressure differences Δp_i and average stagnation pressure $\frac{\rho}{2} u_0^2$. The effect of the groove crest continuing behind the drill hole as downstream roughness is reduced by the "wind shadow" of the groove crest ending in front of the drill hole (see Polzin). Thus as roughness, primarily we have the lateral bounds of the drill hole lying in most cases asymmetrical to the grooves. Thus, according to measurements by Polzin, the errors in pressure measurement are indifferent and one can assume that they are normally distributed. With this assumption, it follows that the measured points p_i are statistically distributed about the true line. Thus, the confidence interval can be reached where the true pressure drop has a 95% probability of residing (Kreyszig 1977). This calculation was performed for several pressure drops on R1, R103 and R105; for R2 such a calculation did not seem useful since only a small number of drill holes gave measured pressure values for statistical evaluation. The length of the confidence was expressed in percent of the pertinent pressure drop $\frac{\Delta p}{I}$ and the pressure drops from various Reynolds number regions were averaged. In this manner there results a percentage deviation for the pressure drops:

in tube R1	0.6%
in tube R103	1.1% and
in tube R105	1.3%

4.2.3 Measurement of Diameter and Its Definition for Grooved Tubes

Since the diameter goes into the formula (4.6) for λ as a fifth-power factor, its measurement requires particular attention. First, the diameter of the smooth tube was determined with an inside micrometer. For the grooved tubes, the diameter $2r_I$ was determined on the groove crests, also with the inside micrometer whose wide contact points extended over several grooves. The data are found in section 3.2 together with standard deviation; the maximum deviation from the average is a measure for the roundness of the tubes. The shape and height of the grooves was measured and photographed under a microscope as described in section 3.2. In figure 4/9 there are four possible definitions for the radius of the grooved tube. The following values result for the various diameters:

	d_I	d_F	d_H	d_A [mm]
R 103	38,20	38,38	38,33	38,46
R 105	42,13	42,55	42,63	43,16

Table 4/1: Size of the Four Possible Diameters of Grooved Tubes, Definition from figure 4/9.

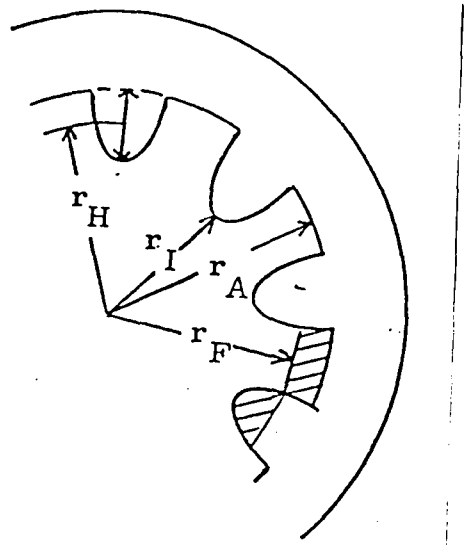

Figure 4/9: Size of the Possible Radii in the Grooved Tubes

r_I : Radius up to the groove crest, directly measurable

r_A : Radius except for the groove valleys = $r_I + h$

r_F : Radius to equivalent surface = $\sqrt{\frac{1}{\pi}(\pi r_I^2 + 240A)}$

r_H : Radius up to half the groove height $r_I + \frac{h}{2}$

Since the 5th power of the diameter comes into being in formula (4.6) because the velocity u_Q is expressed by the flow-through Q and the diameter in the tube cross-sectional surface $\frac{\pi d^2}{4}$, it seemed most expedient to select the diameter d_F of a circular surface equivalent to the total cross-sectional area of the grooved tube. With the standard deviation given in section 3.2, an error of d results which is smaller than 0.05%, for d^5 there results a maximum error of 0.2% with $\left|(\frac{d \pm \Delta d}{d})^5 - 1\right| = 0,002$.

4.2.4 Determination of the Density and Kinematic Viscosity

Density and kinematic viscosity are determined via the equations

$$\varrho = \varrho_o \cdot \frac{p}{p_o} \frac{T_o}{T} \qquad (4.8)$$

and

$$\nu = \frac{\mu}{\varrho}$$

Thus, they are based on a measurement of temperature, pressure and a statement of $\mu(T)$ from the literature. The temperature was measured precisely with a thermometer in front of the calming lane to within 0.1 °C, so the error can be neglected in the formula (4.8) using the absolute temperature. The dynamic viscosity $\mu(T)$ is given in number tables to within 1% (Landolt-Börnstein 1955). For the pressure p, the sum of the average over-pressure in the measuring lane $\frac{p_3}{2}$ and the atmospheric pressure p_o is formed. The error in pressure measurement at drill hole 3 can be neglected, compared to atmospheric pressure; the accuracy of measurement of atmospheric pressure is 0.1%. Thus, there follows $\frac{\Delta\varrho}{\varrho} = 0,1\ \%$ and $\frac{\Delta\nu}{\nu} = 1,1\ \%$.

4.3 Measurement Accuracy for the Coefficient of Resistance λ and the Reynolds Number Re

With the measurement accuracies given in section 4.2 for

the flow-through Q	0.25%
the 5th power of diameter d^5	0.2 %
the density ϱ	0.1 %
the kinematic viscosity ν	1.1 %
the pressure drop for tube R1	0.6 %
R103	1.1 %
and R105	1.3 %

there results a relative maximum error for the

Reynolds number $Re = \frac{Q}{d\nu} \cdot \frac{4}{\pi}$ 1.4 %

and for the coefficient of resistance $\lambda = \frac{\frac{\Delta p}{l} \cdot d^5}{\varrho \cdot Q^2} \frac{\pi^2}{8}$

for the tubes	R1	1.4 %
	R103	1.9 %
	R105	2.1 %

4.4 Results and Discussion

In this section the curves $\lambda = f(Re)$ shall be presented and discussed for smooth and grooved tubes.

4.4.1 Smooth Tubes

a) Tube R1

In the manner described above, average pressure drop per length unit, kinematic viscosity and density for various flows were determined and λ and Re are computed from the formulas (4.6) and (4.7). Figure 4/10 shows the profile of the curve $\lambda = f(Re)$ on a double-log scale. A line results which is determined by the method of smallest error quadrants as:

$$\lambda_{R1} = 0,3454 \cdot Re^{-0,260} \qquad (4.8)$$

b) Tube 2

Similarly, for tube R2 we have:

$$\lambda_{R2} = 0,3426 \cdot Re^{-0,259} \qquad (4.9)$$

There results a quite good agreement of the two tubes, even though they are made of different materials (aluminum and PVC) and thus in general, have different surface roughness. In figure 4/11 we find measured values for tube 2 and the compensation line through measured points of both tubes:

$$\lambda_{R1/R2} = 0,3435 \cdot Re^{-0,259} \qquad (4.10)$$

With the Blasius law (4.3) there also results a good correlation:

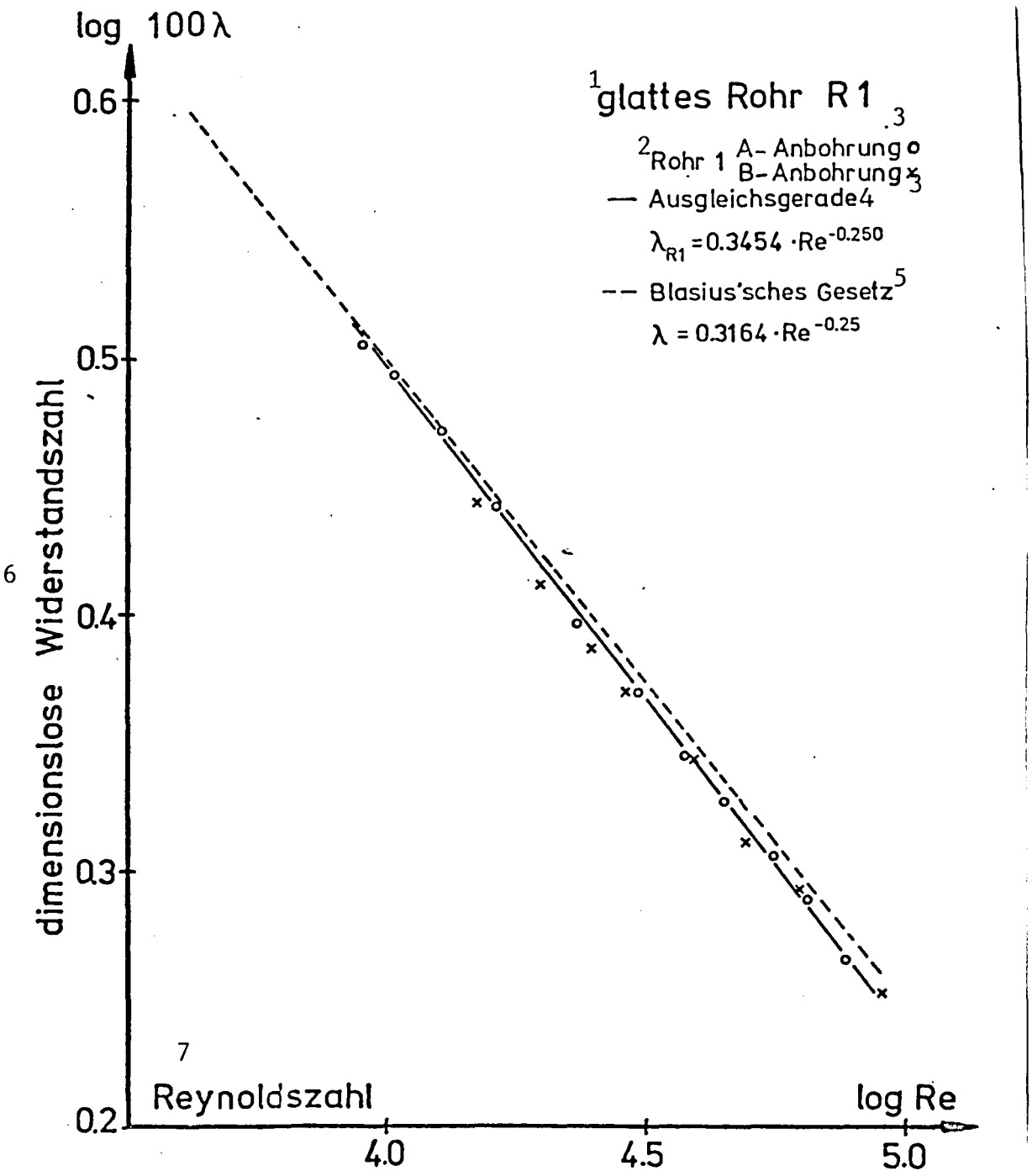

Fig. 4/10: Resistance Law for the Smooth Tube R1

Key: 1-smooth tube 2-tube 3-drilled hole 4-compensation line 5-Blasius law 6-dimensionless coefficient of resistance 7-Reynolds number

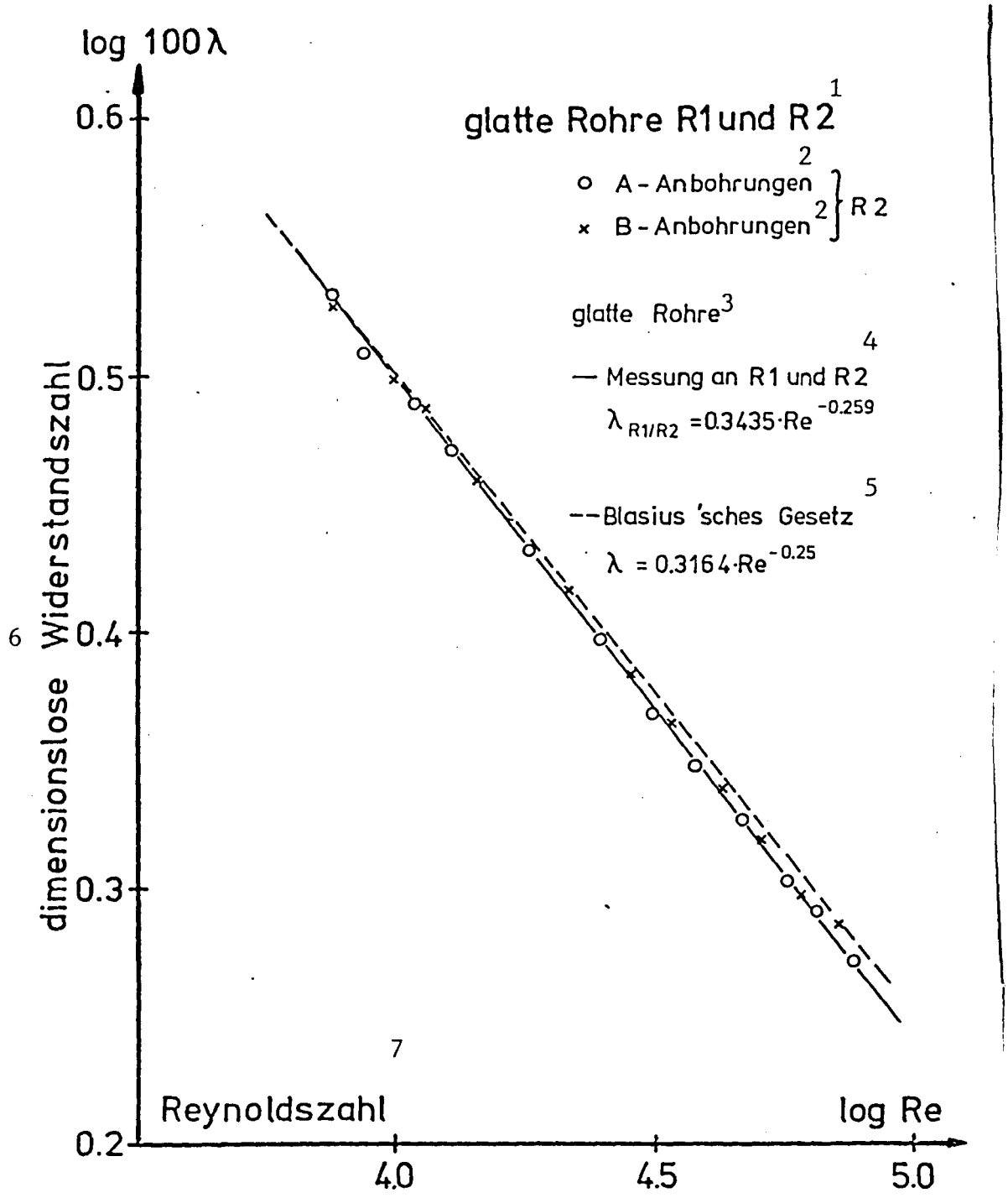

Fig. 4/11: Resistance Law for Smooth Tubes R1 and R2

Key: 1-smmoth tubes R1 and R2 2-drilled holes 3-smooth tubes 4-measurement of R1 and R2 5-Blasius' law 6-dimensionless coefficient of resistance 7-Reynolds number

$Re \cdot 10^{-4}$	$100\lambda_{Blasius}$	$100\lambda_{R1/R2}$	$\frac{\lambda_{Blasius}}{\lambda_{R1/R2}}$
0,7	3,459	3,468	0,997
1,0	3,164	3,162	1,001
3,0	2,404	2,379	1,011
8,0	1,881	1,845	1,019

Table 4/2: Comparison of Resistance Values from Blasius' Law and the Law Found Here (4.10).

In the region of larger Reynolds numbers the computed curve $\lambda = f(Re)$ here lies under the law given by Blasius. However, the deviations remain within the Blasius error limit of $\pm$ 2% (Blasius 1913, Fromm 1923).

4.4.2 Grooved Tubes

As described in section 4.2.2, the pressure drops per length unit were determined with the pertinent flow-through. The coefficient of resistance and the Reynolds number Re were computed from this; as diameter of the grooved tube, d_F is used. Figures 4/12, 4/13 result for tubes R103 and R105. The drawings suggest a division of measured values into three regions: A region of small Reynolds numbers $Re < 10^4$ or $Re < 8 \cdot 10^3$, in which the coefficients of resistance are scattered about the compensation line of measured values for the smooth tube; a middle region of Reynolds numbers $10^4 < Re < 45 \cdot 10^3$ or $8 \cdot 10^3 < Re < 28 \cdot 10^3$, in which the coefficient of resistance is smaller than for the smooth tube, and a region of larger Re numbers $Re > 45 \cdot 10^3$ or $Re > 28 \cdot 10^3$, in which λ increases ever faster than the coefficient of resistance for the smooth tube with rising Reynolds number. In order to have a comparison with the hypothesis developed in chapter 2, figures 4/12 and 4/13 contain an additional log Re scale (besides the $b^+ = b \frac{u_\tau}{\nu}$) with b as the distance between groove crests. The dimensionless groove height h^+ results by multiplication with the factors $\frac{h}{b}$ ($\frac{h}{b} = 0.26$ for R 103, $\frac{h}{b} = 0.86$ for R105). In figures 4/14 and 4/15, another plot was chosen for illustration. The change in resistance ΔW is defined as:

$$\Delta W = \frac{\lambda_{Rillen} - \lambda_{R1/R2}}{\lambda_{R1/R2}}$$

The horizontal, dashed lines show the greatest-possible fluctuation in resistance values for the smooth tubes. In these figures we see more clearly the division into three regions as specified in table 4/3.

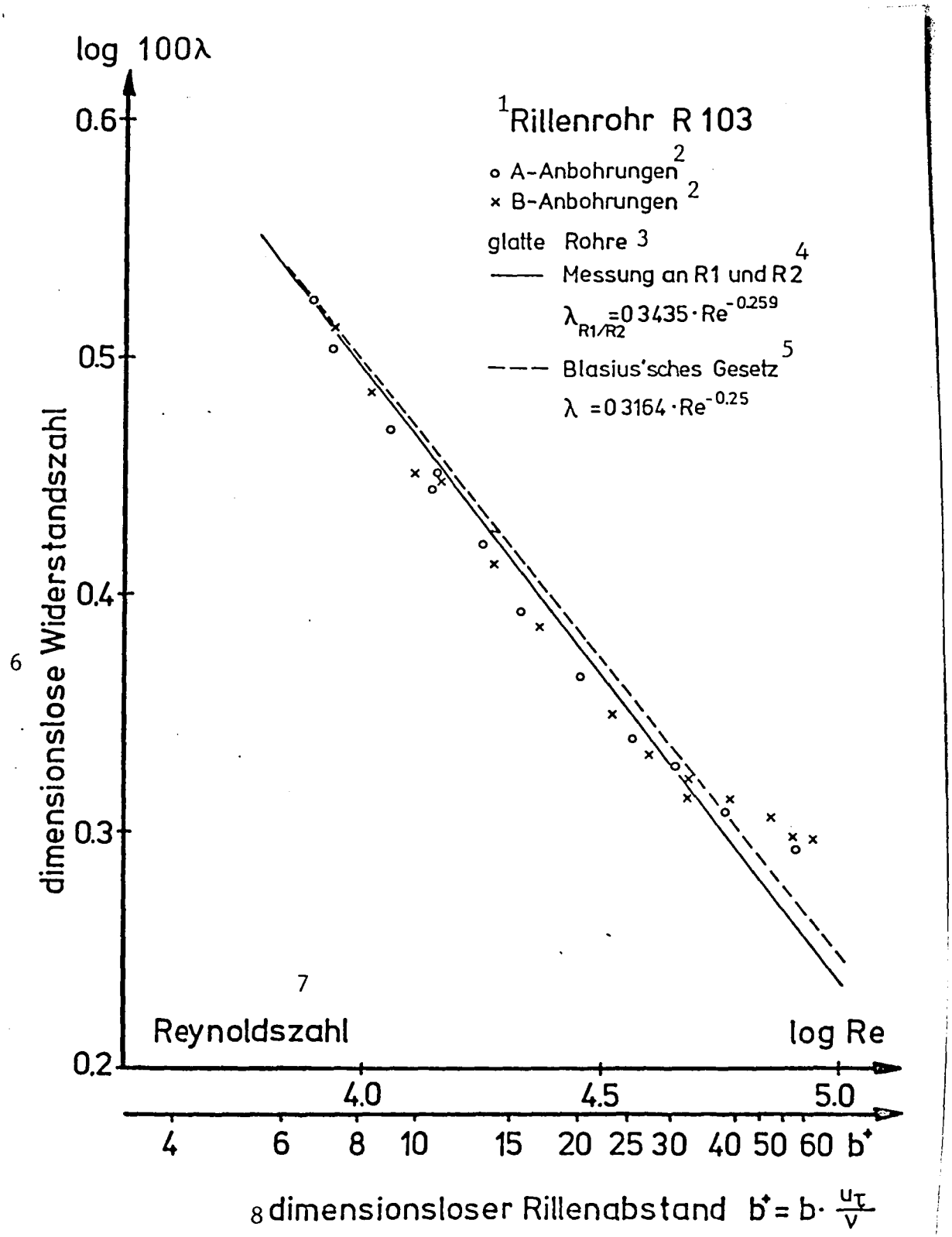

Fig. 4/12: The Resistance Law for Grooved Tube R103

Key: 1-grooved tube 2-drilled hole 3-smooth tube 4-measurement of R1 and R2 5-Blasius' law 6-dimensionless coefficient of resistance 7-Reynolds number 8-dimensionless groove spacing

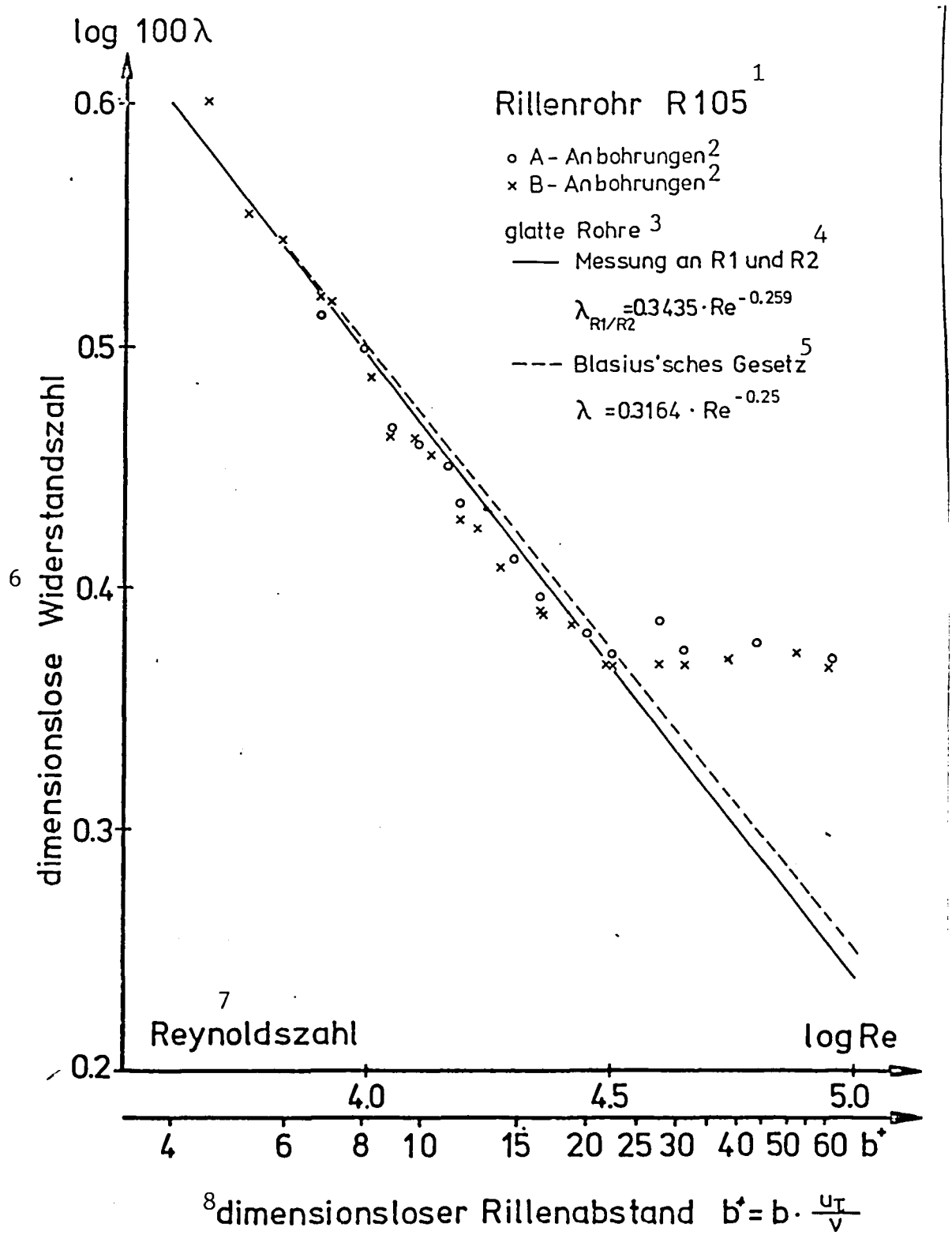

Fig. 4/13: The Resistance Law for Grooved Tube R105

Key: 1-grooved tube 2-drilled hole 3-smooth tube 4-measurement of R1 and R2 5-Blasius' law 6-dimensionless coefficient of resistance 7-Reynolds number 8-dimensionless groove spacing

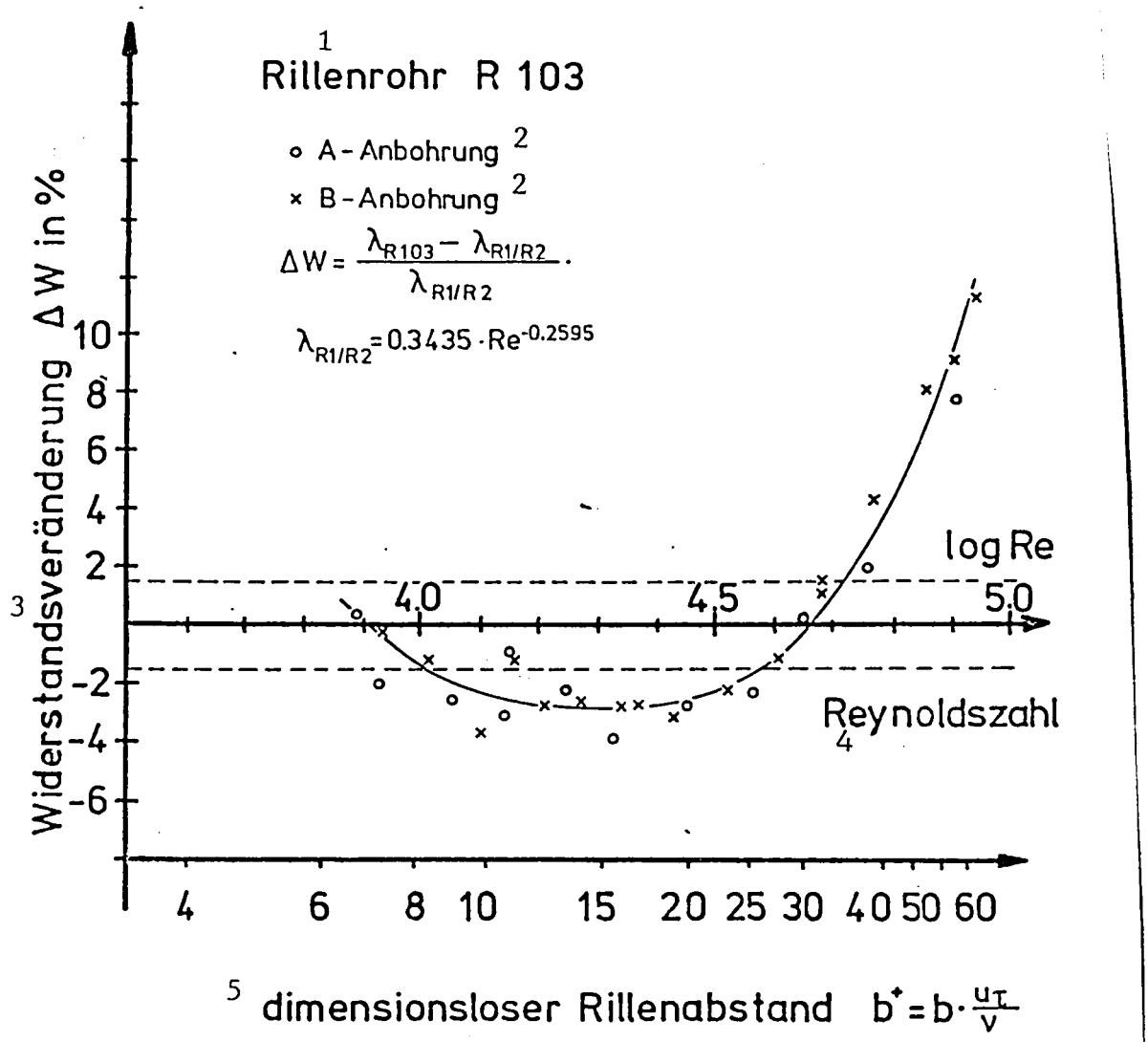

Fig. 4/14: Change in Resistance for Grooved Tube R103 compared to The Results on Smooth Tube, as a Function of Reynolds number and dimensionless groove width b^+.

Key: 1-grooved tube 2-drilled hole 3-change in resistance 4-Reynolds number 5-dimensionless groove spacing

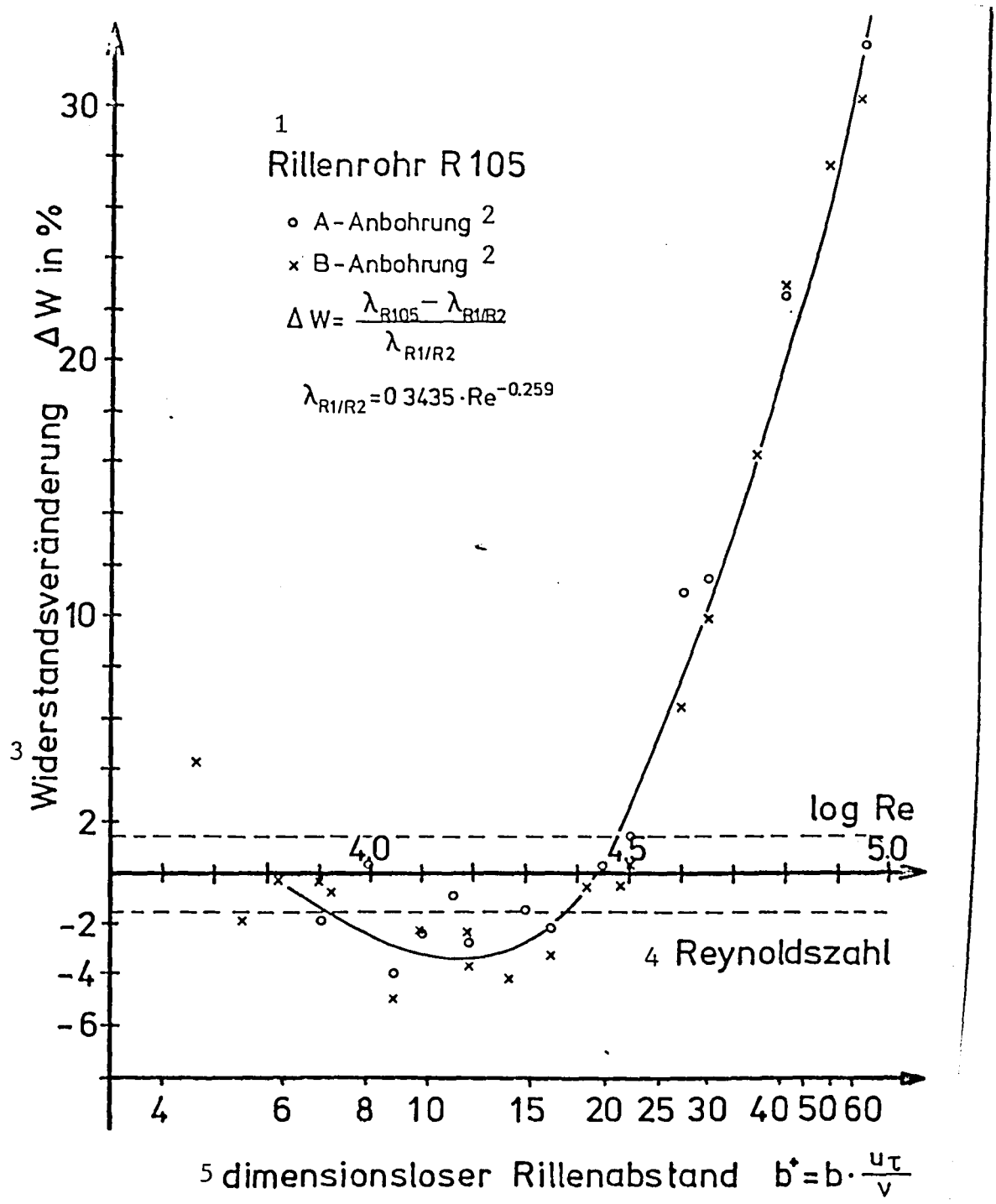

Fig. 4/15: Change in Resistance for Grooved Tube R105 Compared to the Results on Smooth Tube, as a Function of Reynolds Number and Dimensionless Groove Width b^+.

Key: 1-grooved tube 2-drilled holes 3-change in resistance 4-Re No. 5-dimensionless groove spacing

		$\lambda_{Rillen}^{1} = \lambda_{R1/R2}$	$\lambda_{Rillen}^{1} < \lambda_{R1/R2}$	$\lambda_{Rillen}^{1} > \lambda_{R1/R2}$
R 103	$Re \cdot 10^{-4}$	0,8-1,0	1,0-4,5	4,5-8,0
	b^+	6-8	8-30	30-60
	h^+	1,6-2	2-7,8	7,8-15
R 105	$Re \cdot 10^{-4}$	0,55-0,8	0,8-2,8	2,8-8,0
	b^+	4,5-8	8-20	20-50
	h^+	3,9-6,9	6,9-17,2	17,2-43

Table 4/3: Division into Three Regions due to Change in Resistance, Compared to Results on Smooth Tubes

Key: 1-grooves

The size regions of dimensionless groove height h^+ for decreased resistance hardly coincide for the two grooved tubes. For tube R105 $h^+ > 5$ and the resistance must be increased compared to the smooth tube. For tube R103, h^+ is around 5 and so in this region, at least for higher Reynolds numbers, a slight increase in resistance should show up. With groove height h^+ it is not possible to characterize the similar behavior of the two curves. Prandtl's ideas on roughness flow for longitudinal grooves also do not seem to be valid. However, the regions b^+ for both tubes coincide quite well and also coincide with the lower region b^+ which was computed for the grooves on the shark scale in section 2. In this region $b^+ = 8...20...30$, the resistance of the grooved tube shows a reduction by about 3% in the minimum of the curve, in spite of the severe surface enlargement (50% for R103 and 100% for R105).

As mentioned in section 4.2.3, the coefficient of resistance λ increases with the 5th power of the diameter (formula 4.6). For a presentation of the results, the most reasonable-appearing diameter was chosen for the equivalent surface d_F. With the selection of another diameter for the grooved tubes, the results of the change in resistance also change compared to the smooth tubes. For this reason, table 4/4 shows which change in resistance ΔW occurs in the minimum of the curves in figures 4/14 and 4/15 with the other diameters from figure 4/9.

R 103		R 105	
Durchmesser l mm	ΔW %	ΔW %	Durchmesser l mm
d_F = 38,38	-3,0	-3,0	d_F = 42,55
d_A = 38,46	-2,0	+3,8	d_A = 43,16
d_I = 38,20	-5,3	-7,7	d_I = 42,13
d_H = 38,33	-3,6	-2,1	d_H = 42,63

Table 4/4: Change in $\Delta W = \frac{\lambda_{Rillen} - \lambda_{R1/R2}}{\lambda_{R1/R2}}$ due to a Different Selection of the Diameter of Grooved Tubes.

Key: 1-diameter

5. Profile of Average Velocity $\bar{u}$ and of the Effective Value of the Velocity Fluctuations u'_{rms}

5.1 Introduction

In the following chapter, the measurements of the velocity profile $\bar{u}(y)$ and of the profile of the effective value of u' on smooth tubes are presented, related to other investigations and compared in a second section with the results from the grooved tubes. In order to do this, several results from other experimentors are presented and some theoretical considerations are presented.

For a dimensionless plot of the velocity profile, Nikuradse (1932) found the following empirical relation:

$$\frac{\bar{u}}{u_M} = \left(\frac{y}{r}\right)^{1/n} \qquad (5.1)$$

According to these measurements, the factor n increases exponentially from 6 to 10 for Reynolds numbers increasing from $4 \cdot 10^3$ to $32 \cdot 10^6$.

From similarity and dimensional considerations, a theoretical law can be developed which is valid especially in near-wall regions. In near-wall regions the quantities of kinematic viscosity ν, wall shear stress τ_w, density ϱ and wall separation y essentially all have an influence on the velocity. As a simple and meaningful combination of these quantities, we have:

$$\bar{u} = u_\tau \cdot f\left(\frac{u_\tau \cdot y}{\nu}\right) \qquad u_\tau = \sqrt{\frac{\tau_w}{\rho}}$$

$$u^+ = \frac{\bar{u}}{u_\tau} = f(y^+) \qquad (5.2)$$

so that

In the viscous sublayer where the fraction of turbulent shear stress $-\rho\overline{u'v'}$ is very small compared to the viscous stress, $\rho\overline{u'v'} \ll \mu\frac{d\bar{u}}{dy}$, the form of the law can be written down immediately. Because with τ in the viscous sublayer:

$$\tau_w = \mu\frac{du}{dy} \approx \mu\frac{u}{y}$$

and otherwise

$$\tau_w = \rho u_\tau^2$$

there follows

$$u^+ = \frac{\bar{u}}{u_\tau} = y^+$$

According to the Prandtl mixed path law for near-wall region (Schlichting 1965, p. 546), we can write:

$$\frac{d\bar{u}}{dy} = \frac{1}{\varkappa}\frac{\bar{u}}{y} \qquad (5.3)$$

Thus we have:

$$\frac{1}{\varkappa} = \frac{y}{\bar{u}} \cdot \frac{d\bar{u}}{dy} = y \cdot \frac{u_\tau}{\nu} \cdot \frac{df}{dy^+} = y^+ \cdot \frac{df}{dy^+}$$

and as universal wall law there follows:

$$u^+ = \frac{\bar{u}}{u_\tau} = \frac{1}{\varkappa}\ln y^+ + C \qquad (5.4)$$

C: Integration constant

Since this law was developed as a wall-law, it applies for all near-wall turbulent flows. For tube flow it applies in particular far out into the middle, since even in the middle range, the velocity is determined via the pressure drop by means of

$$u_\tau = \sqrt{\frac{\Delta p}{l} \cdot \frac{r}{2\rho}}$$

	Strömungs-medium 1	Kanal-form 2	Reynolds-zahl 3	$\frac{u'_{rms}}{u}$ 4in Rohr-Kanalmitte	$\frac{u'_{rms}}{u}$ 5 im Maximum	Maximum 6 bei y^+
Langeheineken (1981)	7 Luft	8 Rohr	$0,74 \cdot 10^4$	0,8	2,53	14
Laufer (1955)	7 Luft	8 Rohr	$5 \cdot 10^4$ $50 \cdot 10^4$	0,75 0,85	2,6	14
Schildknecht (1975)	7 Luft	8 Rohr	$1,7 \cdot 10^4$	0,8	2,7	14
Lawn (1971)	7 Luft	8 Rohr	$0,85\text{-}1,6 \cdot 10^4$	0,95	-	-
Kreplin (1976)	9 Öl	10 Kanal	$0,77 \cdot 10^4$	0,85	2,9	14
Hofbauer (1978)	9 Öl	10 Kanal	$0,81 \cdot 10^4$	0,85	2,9	14

Table 5/1: Compilation of Investigations of the Effective Value of the Velocity Fluctuations in the Flow Direction

Key: 1-flow medium 2-channel form 3-Reynolds number 4-in middle of tube-channel 5-in the maximum 6-maximum at 7-air 8-tube 9-oil 10-channel

On rough tubes, the same assumptions apply as for the smooth tube (5.3), so that the same velocity law can be developed. However, the constant C_u changes as a function of the dimensionless roughness height $h^+ = h \frac{u_\tau}{\nu}$.

In table 5/1 there are several authors' findings on effective value profiles on tubes and channels. Besides flow medium and channel form, the Reynolds numbers of the measurement and the measured values in the tube or channel medium and in the maximum of the obtained profil are given. The maximum for all measurements lies at $y^+ \approx 14$. In section 5.3, these measurements will be used for comparison purposes.

5.2 Measurement Method and Accuracy

a) The Hot-Wire Probe and Electronic Circuitry

To measure the average velocity $\bar{u}$ and the speed of fluctuation u', a hot-wire with the dimensions shown in figure 5/1 was used in the circuit shown in figure 3/6.

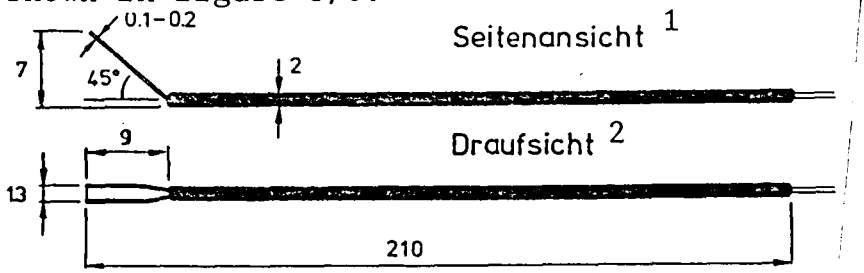

Figure 5/1: Dimensions of the Hot-Wire Probe (mm)

Key: 1-side view 2-top view

The hot wire consists of a 5 µm-thick tungsten wire. As superheating ratio:

$$\alpha = \frac{\text{Warm resistance}}{\text{Cold resistance}}$$

the value 1.8 was chosen in order to have sufficient sensitivity. This superheating ratio corresponds to a temperature difference between hot wire and air of 200 °C.

b) Calibration of Hot-Wire Probe and Measurement of Average Velocity $\bar{u}$

The hot-wire probe was set in the middle of the tube about 10mm in the flow direction in front of a pitot tube (inside diameter d = 0.7 mm) and about 1.5 diameters in front of the tube end. For a calibration curve, the average anemometer stress E_A and the stagnation pressure at the pitot tube $\overline{\frac{\rho}{2} u^2}$ were measured simultaneously.

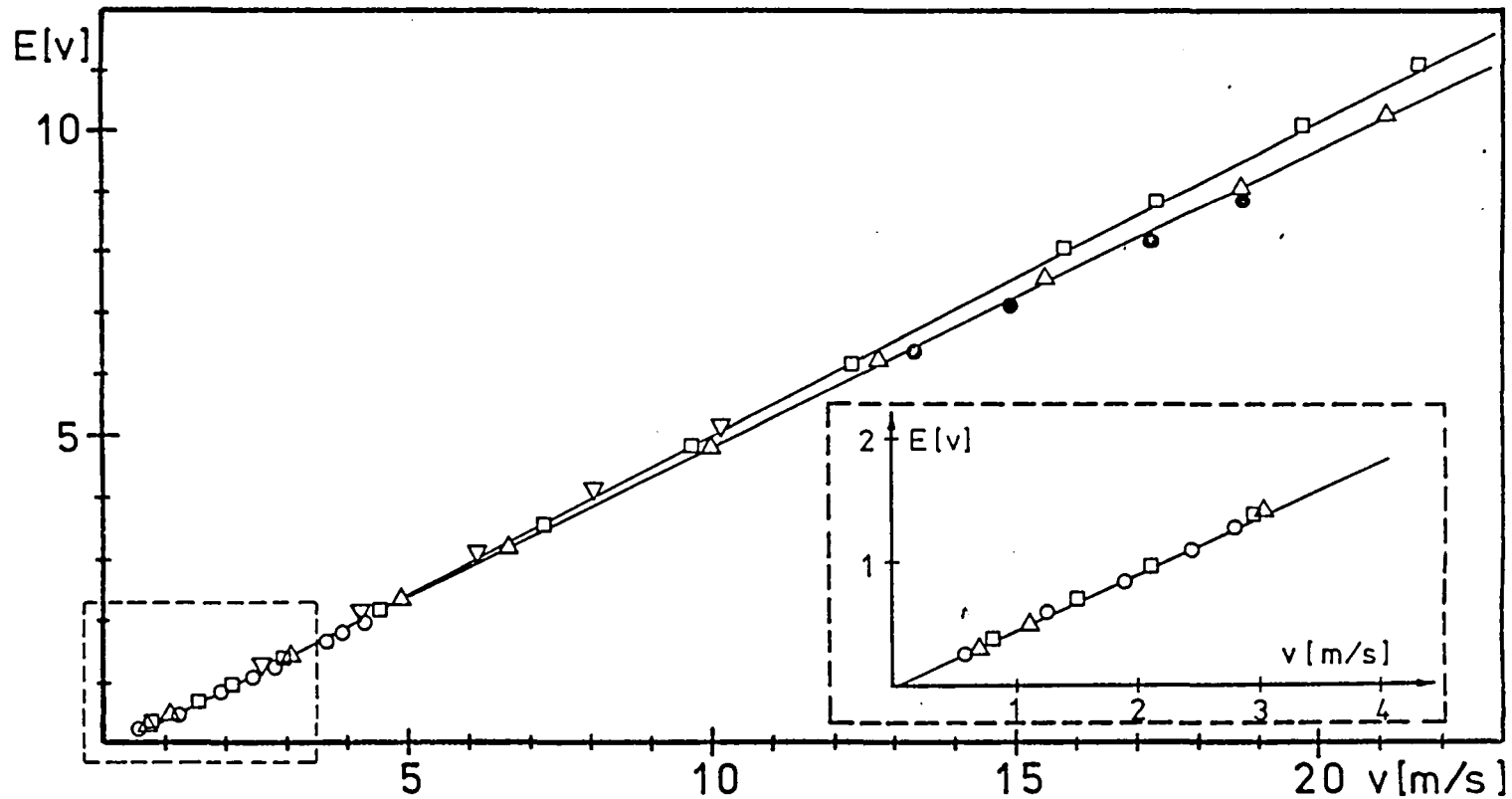

Figure 5/2: Calibration Curve for the Hot Wire with a Cut-out for Smaller Velocities. Various symbols belong to the different measurement series.

In the measurement of the average stagnation pressure, an error is made compared to $\frac{\varrho}{2}\bar{u}^2$, since the fluctuations u' go into the measured value $\overline{\frac{\varrho}{2}u^2} = \frac{\varrho}{2}(\bar{u}^2 + \overline{u'^2})$ as a square. With $\frac{u'_{rms}}{u_\tau} \approx 0,9$ (fig 5/7) and $\frac{u_\tau}{u_M} \approx 4,8\ \%$ (table 5/2) in the tube middle, the fluctuations amount to a maximum 5% of the average velocity. Thus we have:

$$\overline{\frac{\varrho}{2}u^2} = \frac{\varrho}{2}(1 + 0,0025)\,\bar{u}^2$$

This error is thus negligible. The obtained curve $\bar{u} = f(E_A)$ was linearized with the linearizer. This linearized calibration curve was checked repeatedly (figure 5/2). For various measured series it exhibited slightly different slopes (different symbols in figure 5/2). So, before each measurement, a new calibration curve was prepared so that a greater accuracy can be attained. For velocities $\bar{u} > 1.5$ m/s, an error of 2% can be used. In the region of smaller velocities $\bar{u} < 1.5$ m/s, a greater inaccuracy of 2 to 10% pervailed; this number increases with decreasing velocity since a more accurate linearization over more than one order of magnitude is not possible with the linearizer used here.

c) Measurement of the Effective Value of the Velocity Fluctuations u'_{rms}

To measure the effective value u'_{rms} of the velocity fluctuations u', the circuitry already shown in figure 3/6 was used. The FFT analyzer digitalized the recorded output voltage of the linearizer and made a Fast Fourier Transformation in the region of 1.25 Hz to 2001.25 Hz. In figure 5/3, a spectrum of the velocity fluctuations is shown in the tube middle for tube 1 at $Re = 2.5 \cdot 10^4$. At 2000 Hz the fluctuations have already dropped off by 20 dB so that the determination of fluctuations up to 2000 Hz is sufficient. The obtained, instantaneous spectra are then averaged and after measuring times of 80 seconds, after which the changes in results were negligible, they are integrated to a voltage E'_{rms}. E'_{rms} can be converted into the effective value of the velocity fluctuations u'_{rms} by means of the calibration curve. The relative error in u'_{rms} measurement is at 3% for velocities $\bar{u} > 1.5$ m/s. In the lower velocity region, the error is determined by the inaccuracy of the calibration curve of 5 - 10%. In addition to these errors there is a systematic error due to the dimensions of the hot wire. At a length l of the hot wire of 1.3 mm, there results a length in dimensionless units of $l^+ = 7$, $l^+ = 41$, $l^+ = 75$ for the velocities u_M of 2 m/s, 12 m/s and 22 m/s respectively, with $u = 0.04\ u_M$. In the y-direction the effective value of the velocity fluctuations changes near the wall within several y^+ units, so that one can assume that the extent of the turbulence balls in the y- and z-direction lies on this order. At higher velocities then, quite

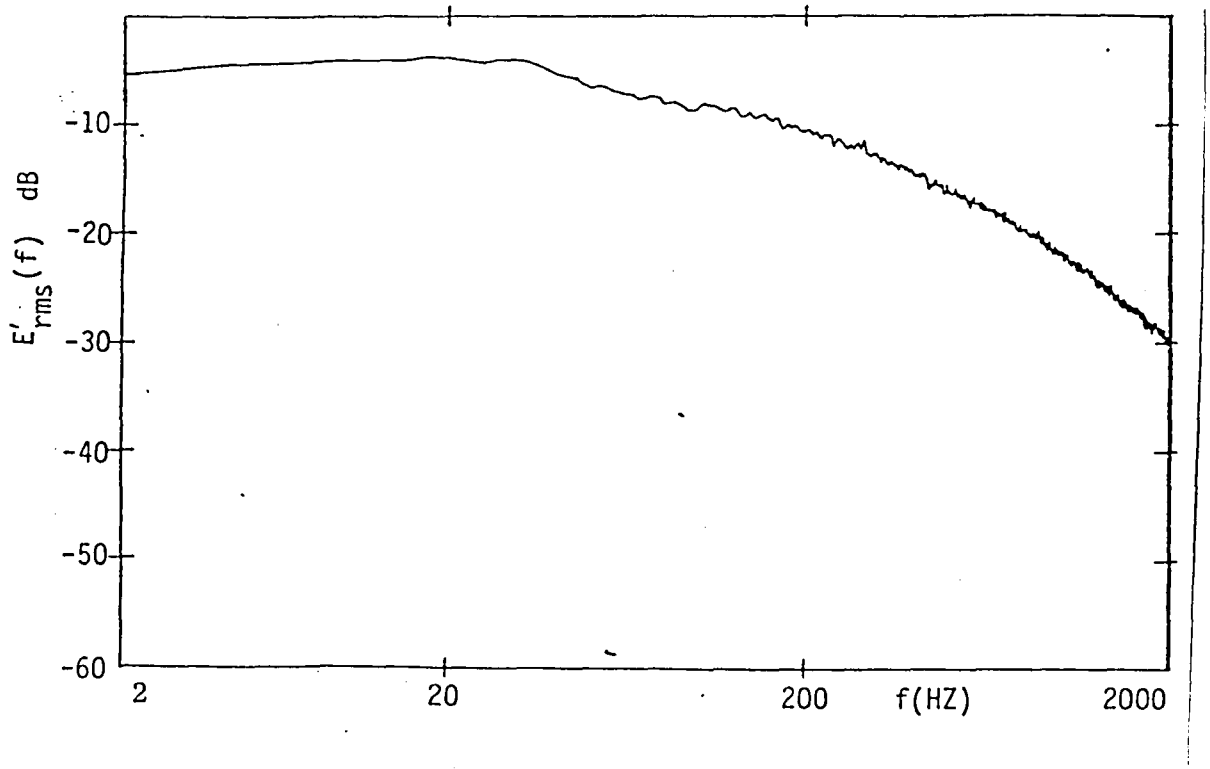

Fig. 5/3: Frequency Spectrum of the Output Voltage of the Linearizer E. Given: The effective value E'_{rms} as a function of the band middle frequency f, bandwidth 2.5 Hz, 800 bands, 0 dB corresponds to $140 \cdot 10^{-3}$ V, $E'_{rms} \quad u'_{rms}$.

different processes evolve over the length of the hot wire. Thus, with increasing Reynolds number, a drop in measured effective value u'_{rms} must be expected. In addition, the hot wire of 1.3 mm has about the length of three groove crest spacing. Near the wall, the hot wire will thus average over specific motions for grooved tubes; said motions taking place over groove crest or valley, respectively. Since in this investigation severe deviations were to be investigated between smooth and grooved tubes, this method will suffice.

d) Positioning of the Probes

During the measurements the hot wire was located about 1.5 d upstream from the tube end. The distance y between wall and hot wire was determined by moving the hot-wire probe until it touched the wall. For the smooth tubes, this point could be determined quite accurately by determining the position 'a' on a micrometer screw by looking through a magnifying glass. In the grooved tubes, care was taken by observation with the magnifying glass from various directions, that the parallax between touching groove crests and hot-wire tines disappeared. It is important to note that a positioning error with respect to the true distance y_w can result only in small values y. In this manner an accuracy of 0.05 mm was attained for the smooth tubes. The error for the grooved tubes will be discussed in section 5.3.2.

e) Accuracy of Wall Shear-Stress Velocity u

Since in the following sections, norming plays an important role, especially with u_τ, an estimation of the error of u_τ will be given here. u_τ can be determined in the tube using formula (4.4) via the pressure drop. This drop was measured between drill holes 3 and 5 and averaged. Since the pressure drop from hole 3 to tube end is constant (see section 4.2.2), u_τ also remains constant up to the measurement point. In a measurement of the pressure drop over only two holes, an error estimation for $\frac{\Delta p}{l}$ of max. 3% resulted, thus the relative error of u_τ is 1.5%. A comparison between the values $\frac{u_\tau}{u_M}$ of the measurements here and the results of other authors (table 5/2) confirms this estimation, since within the frame of measurement accuracy of 2% for u_M and 1.5% for u_τ, there is quite good agreement.

$Re \cdot 10^{-4}$	$\frac{u}{u_M}$ [%] Reichardt (1959)	$\frac{u}{u_M}$ [%] Langeheineken (persönl. Mitt.)[1]	$\frac{u}{u_M}$ [%] [2]hier vorgelegte Messungen
1,0	4,8	4,8	4,9
2,5	4,3	4,3	4,4
4,5	-	-	4,2

Table 5/2: Comparison of Values $\frac{\bar{u}_\tau}{u_M}$ of Different Authors with the Measurements Presented Here.

Key: 1-(personal report) 2-measurements presented here

5.3 Results and Discussion

5.3.1 Smooth Tubes

a) Profile of the Average Velocity $\bar{u}$

Figure 5/4 shows three velocity profiles for three Reynolds numbers on both smooth tubes. The profiles for both tubes, identified by circles or ovals, agree well. If we compare values $\frac{\bar{u}}{u_M}$ for the same $\frac{y}{r}$, then one can see how the profiles become fuller with rising Reynolds number.

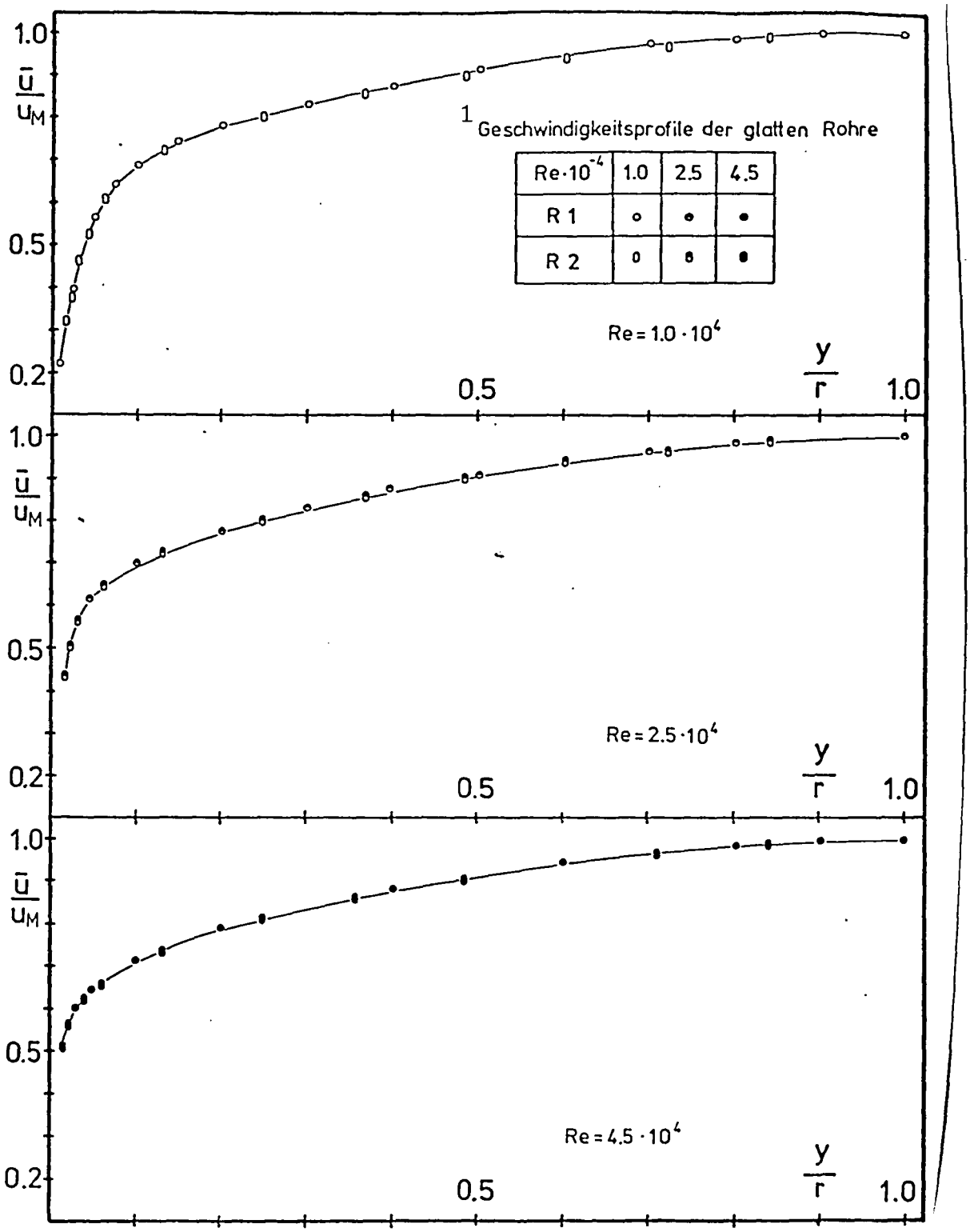

Figure 5/4: Velocity Profile of Smooth Tubes R1 and R2 for Three Reynolds numbers

Key: 1-velocity profile of smooth tubes

In figure 5/5 we see the same profiles on a double-logarithmic plot in order to check the law (5.1)

$$\frac{\bar{u}}{u_M} = \left(\frac{y}{r}\right)^{1/n}$$

mentioned in section 5.1. A comparison of the values n measured here with those of Nikuradse (1932) shows good agreement (table 5/3).

$Re \cdot 10^{-4}$	Messungen [1] Nikuradse n	hier vorgelegte [2] Messungen n
0,4	6,0	
1,0		6,0
2,3	6,6	
2,5		6,6
4,5		6,8
11,0	7,0	

Table 5/3: Comparison of Values n from $\frac{\bar{u}}{u_M} = \left(\frac{y}{r}\right)^{1/n}$ with the Results of Nikuradse (1932).

Key: 1-measurements by Nikuradse 2-measurements presented here

In figure 5/6 a method of plotting is chosen in which the logarithmic wall law is nicely represented. In the region $y^+ = 25$ and $y^+ = 200$, the points are very nicely represented by the line:

$$u^+ = 5,31 \log y^+ + 6,30 \qquad \text{(Curve 1)}$$

In the region $y^+ > 200$, the points deviate upward since the law was developed as a wall-law and thus naturally need not be true in the middle. For $y^+ < 25$, the measured points are lower and roughly correspond to the law valid near the wall:

$$u^+ = y^+ \qquad \text{(Curve 2)}$$

The points $y^+ < 9$ are greatly scattered; therefore an estimation of the error will be provided here. The uncertainty of 0.05 mm cited in section 5.2 in the determination of y gives an uncertainty of Δy^+ for the various Reynolds numbers, as shown in table 5/4.

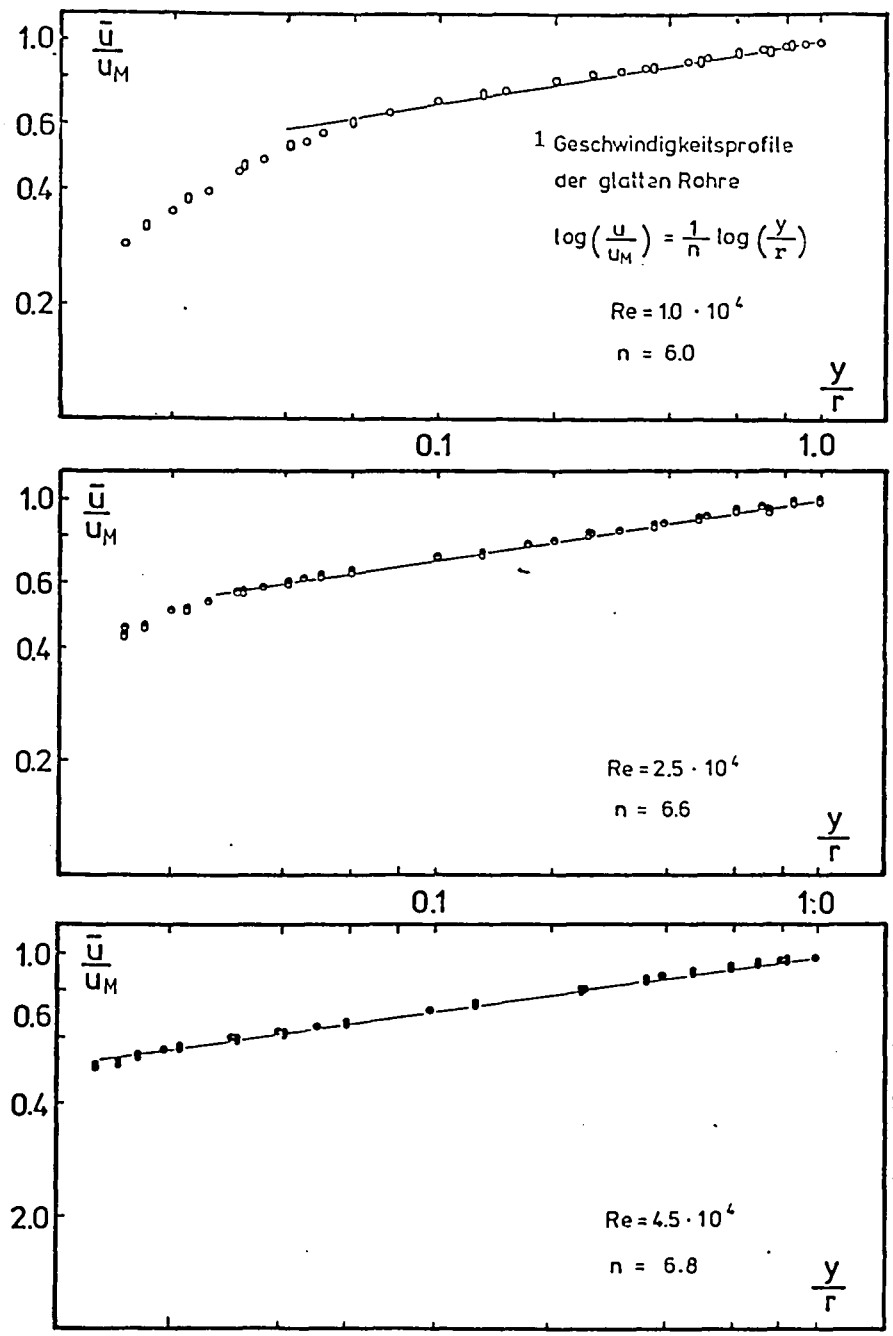

Fig. 5/5: Velocity Profile of Smooth Tubes R1 and R2 for Three Reynolds Numbers Plotted on a Double-Log Scale

Key: 1-velocity profile of the smooth tubes

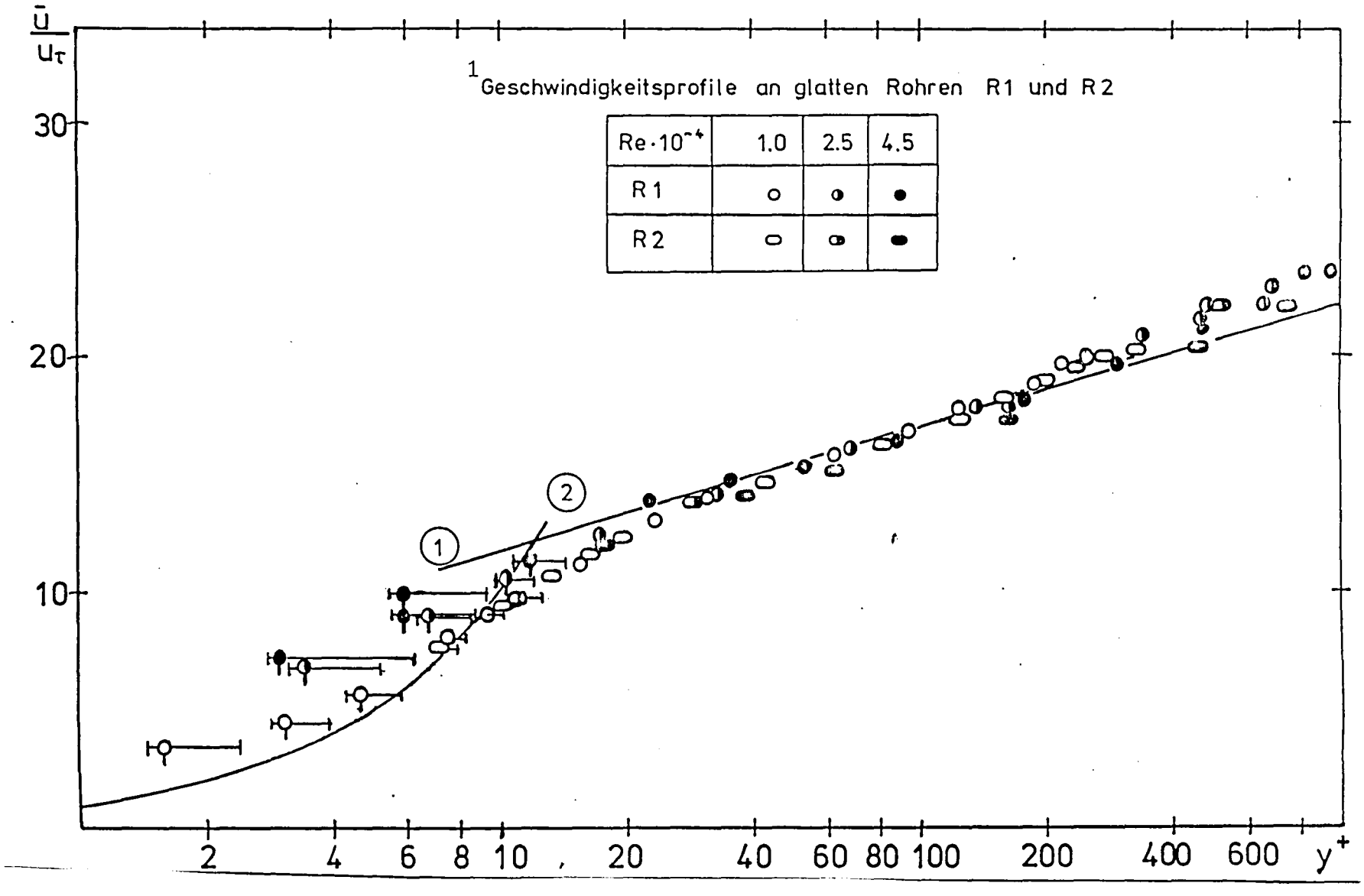

Figure 5/6: Velocity Profile on Smooth Tubes in Dimensionless Units

$1 : u^+ = 5,31 \log y^+ + 6,30, \quad 2 : u^+ = y^+$

Key: 1-velocity profiles on smooth tubes R1 and R2

$Re \cdot 10^{-4}$	1,0	2,5	4,5
u_τ	0,24	0,52	0,91
Δy^+	0,8	1,7	3,0

Table 5/4: Error Δy^+ in y^+ for various Reynolds numbers for an error of 0.05 mm in y with $\nu = 15.3 \cdot 10^6$ m^2/s.

The deviations are entered as error bars. The errors of u_τ are negligible within the framework of this estimation for small values u^+ and y^+. The close proximity to the wall has a greater influence. As Oka (1972) and Graichen (1980) describe, the heat convection on the hot wire increases due to the closeness of the wall and thus evidently also does the velocity. This error occurs for aluminum walls even at greater wall spacing, than for PVC and has a different magnitude for grooved walls as well. Therefore no perpendicular bar is plotted for the estimated error, however, the points for $y \leq 0.3$ mm are indicated by a perpenducular slash.

b) Profiles of the Effective Value of the Velocity Fluctuations u'_{rms}

As described in section 5.2, the effective value was measured. The non-normed values are plotted in figure 5/13 for comparison jointly with the measurements on grooved tubes. But in this section the norming with u_τ is presented and compared with other measurements. Figure 5/7 shows $\frac{u'_{rms}}{u_\tau}$ against $\frac{y}{r}$ and in figure 5/8 as a supplement, the near-wall points are plotted against y^+, again with the error bar for $\Delta y = 0.05$ mm. The values $\frac{u'_{rms}}{u_\tau}$ in the tube middle decrease with increasing Reynolds number, but still lie within the range measured by other authors (table 5/1). In figure 5/7 the maxima lie between $y^+ = 10$ and $y^+ = 15$, in agreement with the mentioned investigations. The size of the maximum decreases, however, with increasing Reynolds number, which is attributable to the length of the hot wire, as discussed above. For the smallest Reynolds number $Re = 1.0 \cdot 10^4$, a comparison with other measurements is shown in figure 5/9. In particular, there is good agreement with the results of Langeheinken (1981). For $Re = 1.0 \cdot 10^4$, the length of the hot wire is still sufficient for resolution of the structures.

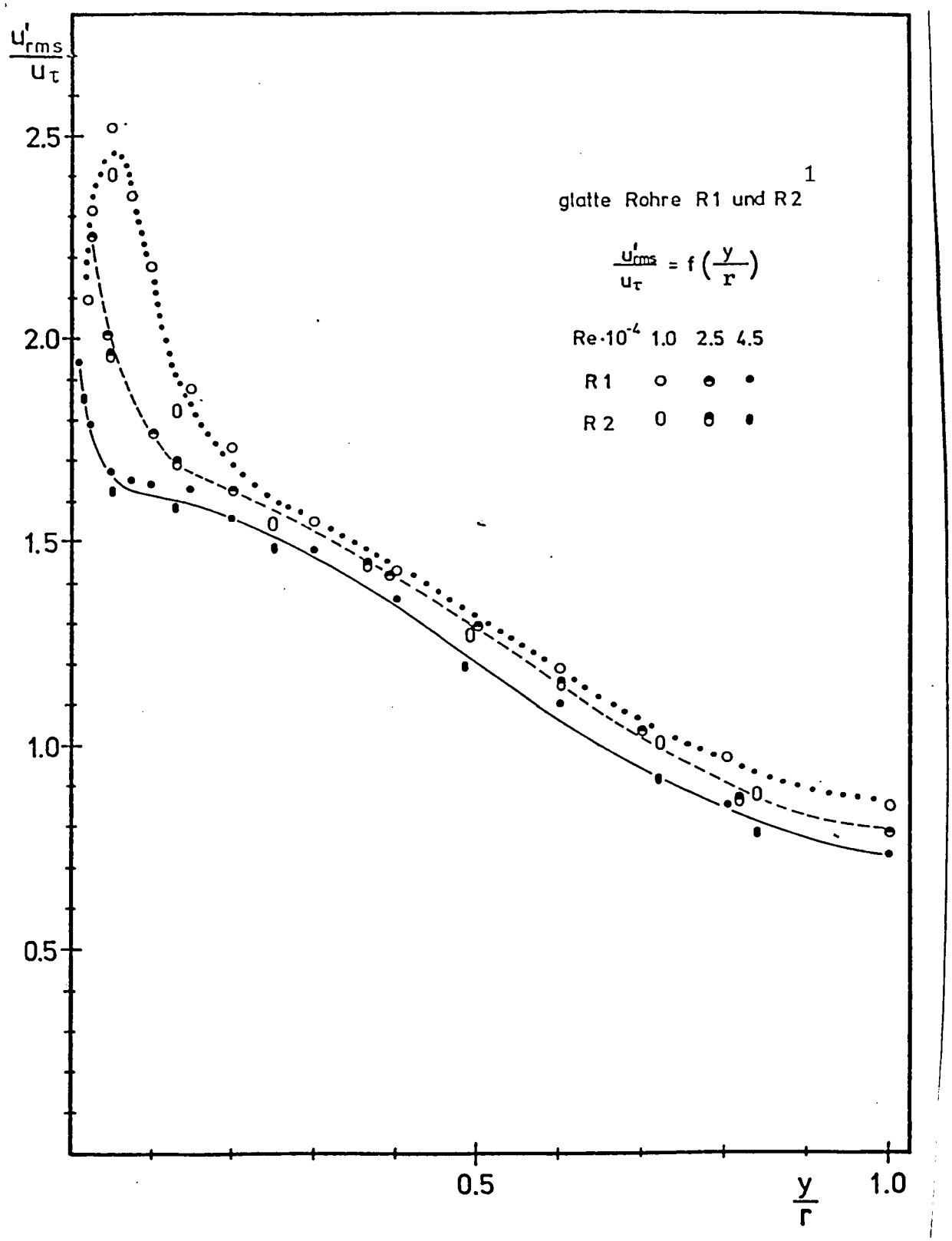

Figure 5/7: Effective-Value Profile $\frac{u'_{rms}}{u_\tau}$ for Smooth Tubes R1 and R2
Key: 1-smooth tubes R1 and R2

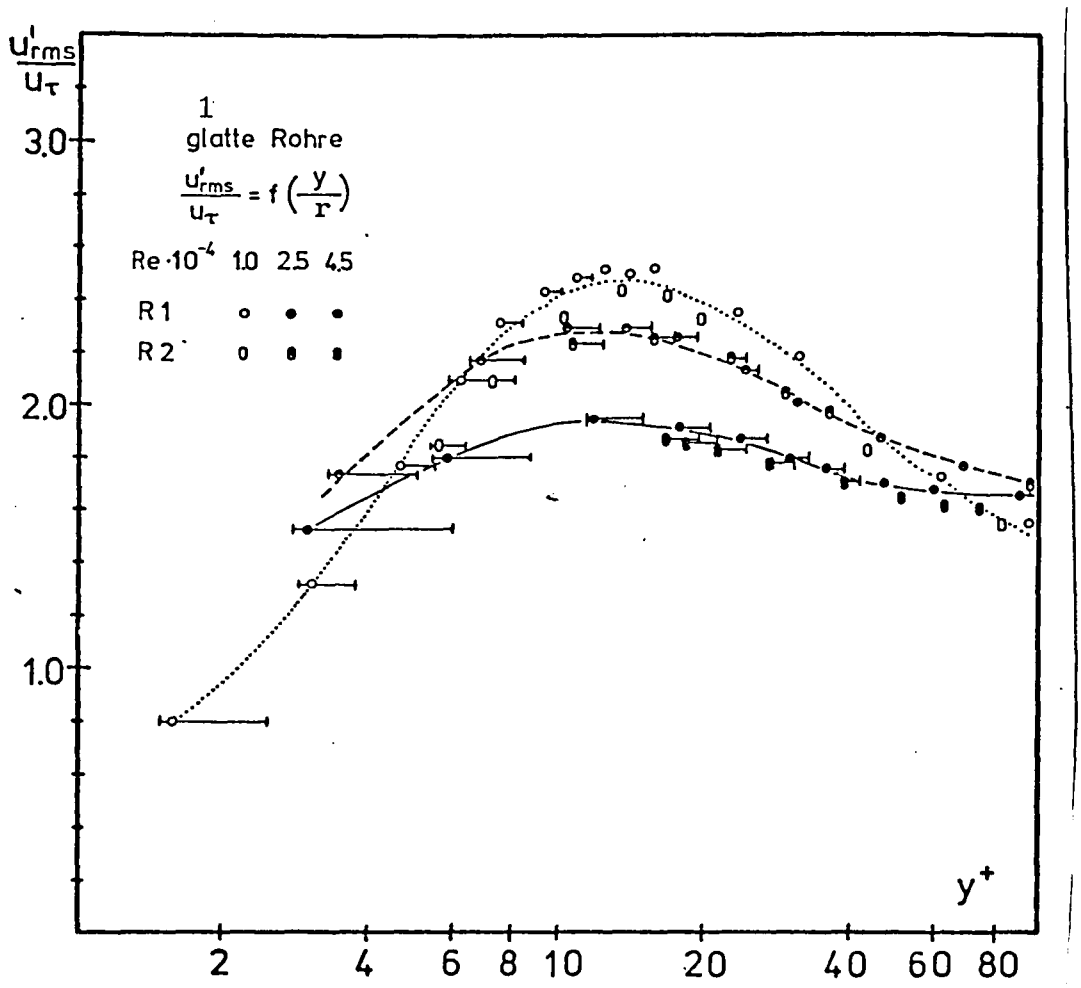

Figure 5/8: Effective-Value Profile of the Smooth Tubes R1 and R2 Plotted Against y^+ Near the Wall

Key: 1-smooth tube

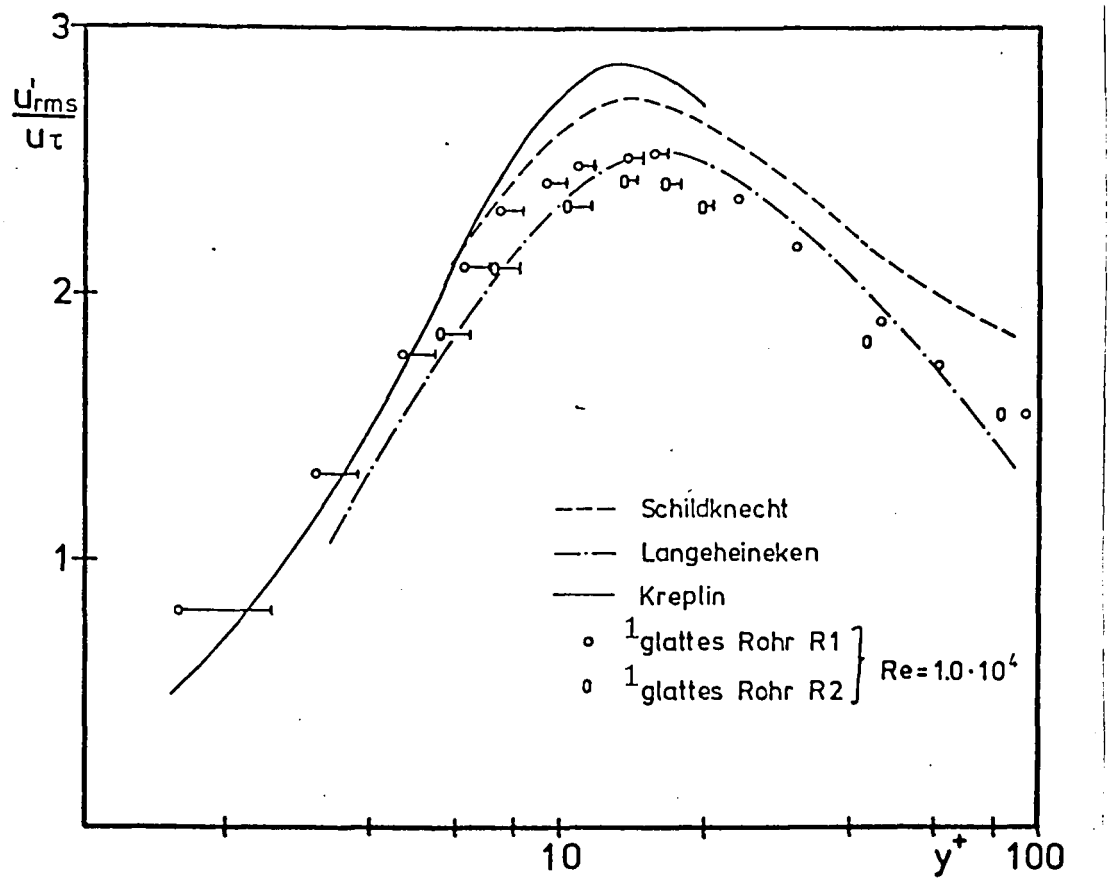

Figure 5/9: Effective-Value Profiles of R1 and R2 Compared with Results of Other Authors

Key: 1-smooth tube

5.3.2 Grooved Tubes

a) Definition of the Zero Point of the y-Axis

Before presenting and discussing the measured results from grooved tubes, it must still be explained what wall separation y is to be defined as the zero point and what changes in other definitions will result therefrom.

As described in section 5.2, the position 'a' was measured against a microscrew to determine where the hot wire contacts the groove crest. If this point is fixed as the zero point $y_I = 0$ of the y_I-axis, then this corresponds to the definition of the radius r_I in figure 4/9. Proceeding from this position, from table 4/1 one can determine the differences $y_A - y_I$, $y_F - y_I$, $y_H - y_I$ in accordance with the definitions of the radii in figure 4/9.

	R 103				R 105			
	Verschiebung in mm	dimensionslose Verschiebung für $Re \cdot 10^{-4}$			Verschiebung in mm	dimensionslose Verschiebung für $Re \cdot 10^{-4}$		
		1,0	2,5	4,5		1,0	2,5	4,5
$y_A - y_I$	0,13	2	4	7	0,52	7	16	30
$y_H - y_I$	0,07	1	2	4	0,25	4	8	14
$y_F - y_I$	0,09	1	3	5	0,21	3	7	12

Table 5/5: Shift of Measurement Points on the y_I-axis due to Different Definition of the zero point. The shifts are dimensionless with the characteristic length of the viscous sublayer $\frac{\nu}{u_\tau}$.

Key: 1-shift in mm 2-dimensionless shift for $Re \cdot 10^{-4}$

The maximum shifts occurring with a different selection of the zero point $\frac{y_A - y_I}{r_I}$, amount to 0.007 for tube R103 and to 0.025 for tube R105. Thus, for $\frac{y}{r} > 0.25$ they can be neglected since in this range, the velocity profile and the profile of effective value have such small ascents that a shift of the zero point causes a change of $\frac{\bar{u}}{u_M}$ or $\frac{u_{rms}}{u_\tau}$, which lies within the error limits. The profiles thus can be represented in a plot against $\frac{y_I}{r_I}$ since y_I was determined

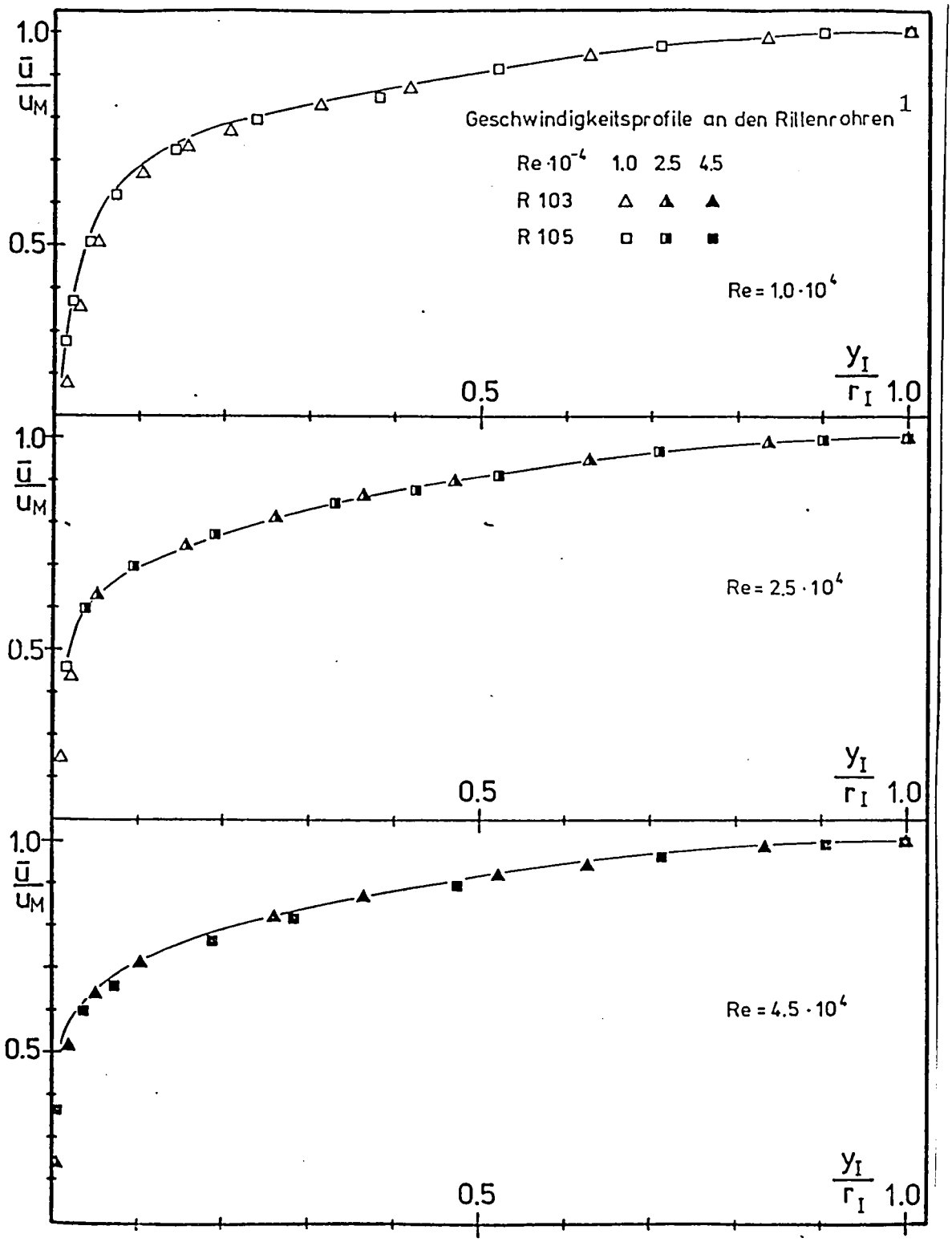

Fig. 5/10: Velocity Profiles of Grooved Tubes R103 and R105 for Three Reynolds numbers; the plotted curves were found for smooth tubes (fig. 5/4).

Key: 1-velocity profiles for grooved tubes

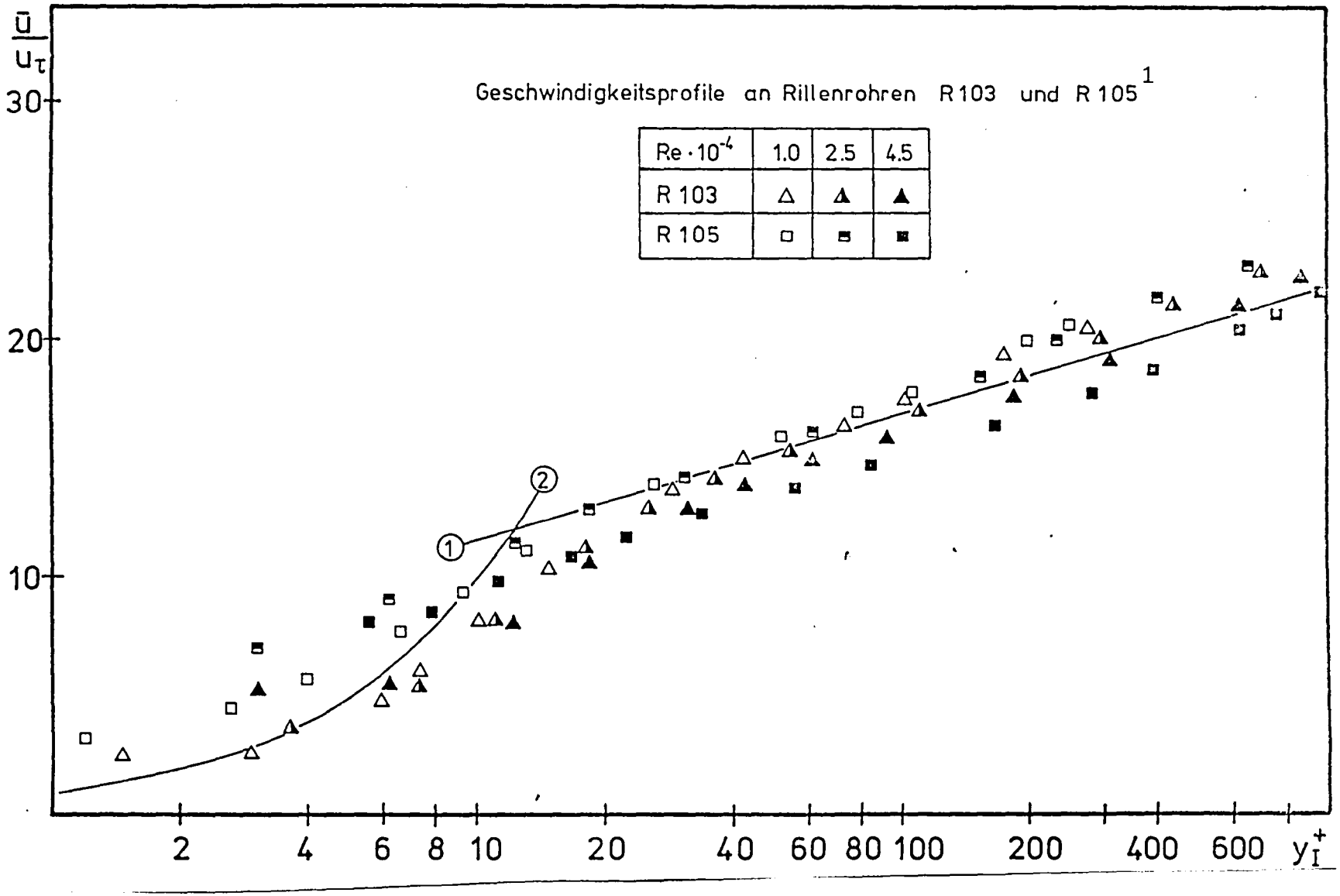

Fig. 5/11: Velocity Profiles of Grooved Tubes in Dimensionless Units
1 : $u^+ = 5,31 \log y_I^+ + 6,30$; 2 : $u^+ = y_I^+$

Key: 1-velocity profiles for grooved tubes R103 and R105

directly. Near the wall, the various definitions should be discussed separately.

b) Profiles of the Average Velocity $\bar{u}$

Figure 5/10 shows the measured velocity profiles of the grooved tubes; for comparison the curves found for the smooth tubes are also included. No differences show up toward the tube middle region, the law $\frac{\bar{u}}{u_M} = (\frac{y}{r})^{1/n}$ thus gives the same values for n for the grooved tubes. Near the wall $\frac{y}{r} < 0.1$, the values $\frac{\bar{u}}{u_M}$ lie somewhat under the curve obtained for the smooth tube. A shift of the zero point would intensity this behavior.

For comparison with the logarithmic wall law found for smooth tubes, figure 5/11 presents the velocity profiles with norming of $u^+ = f(y^+)$ and the line found for the smooth tubes:

$$u^+ = 5,31 \log y^+ + 6.30$$

and for small y^+-values:

$$u^+ = y^+.$$

The measured values for both grooved tubes fit well for Re = $1.0 \cdot 10^4$ and $2.5 \cdot 10^4$ with the line (Curve [1]) found for smooth tubes. For Re = $4.5 \cdot 10^4$ they lie under the line, since for this Reynolds number a greater resistance

$$\lambda = \frac{\frac{\Delta p}{l} \cdot d}{\frac{\varrho}{2} u_Q^2} \qquad \text{and} \qquad u_\tau = \sqrt{\frac{\Delta p}{l} \cdot \frac{r}{2\varrho}}$$

than on the smooth tubes is expected. In table 5/6 the ratio $\frac{u_\tau}{u_M}$

Re · 10^{-4}	R 1 und R 2 glatte Rohre[1]	R 103 Rillenrohre[2]	R 105 Rillenrohre[2]
1,0	0,049	0,049	0,049
2,5	0,044	0,044	0,044
4,5	0,042	0,043	0,045

Table 5/6: Ratio of $\frac{u_\tau}{u_M}$ for Smooth and Grooved Tubes for Three Reynolds Numbers.

Key: 1-R1 and R2, smooth tubes 3-grooved tubes

is entered as a function of the Reynolds number for grooved tubes and smooth tubes. For the two small Reynolds numbers, the values $\frac{u_\tau}{u_M}$ do not differ, for Re = $4.5 \cdot 10^4$, $\frac{u_\tau}{u_M}$ is larger for the grooved tubes.

With larger value u_τ, the points $u^+ = f(y^+)$ shift in the direction of smaller values u^+ and larger values y^+, as shown in figure 5/11. The near-wall points $y_I^+ < 10$ have similar severe scattering as the smooth tubes. The different definitions of the zero point of the y-axis have a much stronger influence on the location of the measurement points than the measured error in the spacing measurement, so that error bars can be omitted. In figure 5/12 the near-wall measured values are plotted against the y-axes defined with various zero point. For the three illustrations, the values $\frac{\bar{u}}{u_\tau}$ for $y^+ < 8$ are too low; for the illustration plotted against y_I^+ (figure 5/11), the results agree approximately with those of the smooth tubes.

c) Profiles of the Effective Value of Velocity Fluctuations u'_{rms}

The profiles $u'_{rms}(y)$ are presented in figure 5/13 as a function of y (non-normed). A qualitative comparison of the curves shows a large similarity in the shape of the curves. There is a striking difference at Re = $4.5 \cdot 10^4$ in the severe reduction of the near-wall maximum of u'_{rms} for grooved tube R105. Quantitative comparisons between smooth and grooved tubes are possible only in the normed representation (fig. 5/14) or for the near-wall region (fig. 5/15). For $y_I^+ > 10$, no severe deviations show up, except for points where Re = $4.5 \cdot 10^4$, which lie under the curves of the smooth tubes. At this Reynolds number u_τ, as described above, is greater for the grooved tubes, and thus $\frac{u'_{rms}}{u_\tau}$ becomes smaller. For $y_I^+ < 10$, there continues to be agreement between the smooth tubes and grooved tubes R105 at Re = $1.0 \cdot 10^4$ and $2.5 \cdot 10^4$. Tube R103 shows however, a stronger drop in $\frac{u'_{rms}}{u_\tau}$ with decreasing y_I^+ than the smooth tube. The normed effective value $\frac{u'_{rms}}{u_\tau}$ on tube R105 remains nearly constant near the wall for Re = $4.5 \cdot 10^4$. In order to demonstrate the influence of the various definitions of the zero point of y on the u'_{rms}-profile, in figure 5/16 the near-wall measured values are plotted for Re= $2.5 \cdot 10^4$ against the three y^+-axes. Again, it turns out that the plot against y_I^+ approximately agrees with results from the smooth tubes; here the maximum of the curves lies at $y^+ \approx 15$, as expected from other investigations (table 5/1).

As a result of this chapter one can state: The velocity profiles of smooth tubes were measured with good agreement with other authors. For $y^+ < 10$, severe deviations turn up in the representation of $\frac{\bar{u}}{u_\tau} = f(y^+)$; these are generated due to heat convection due to

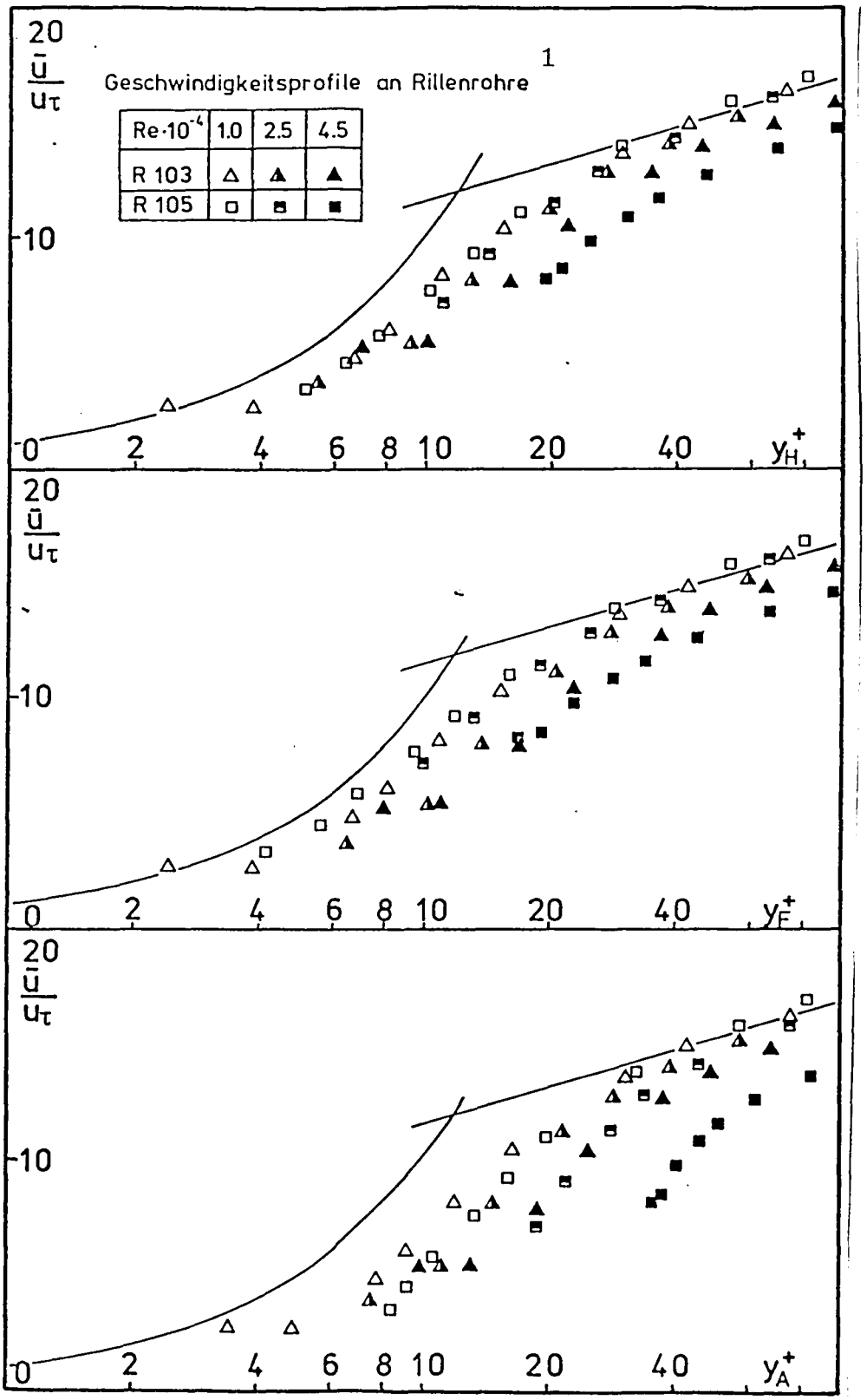

Fig. 5/12: Velocity Profile of Grooved Tubes in Dimensionless Units as Functions of y_F^+, y_H^+ and y_A^+

Key: 1-velocity profiles of grooves tubes

$$1 : u^+ = 5,31 \log y^+ + 6,30; \quad 2 : y^+ = y^+$$

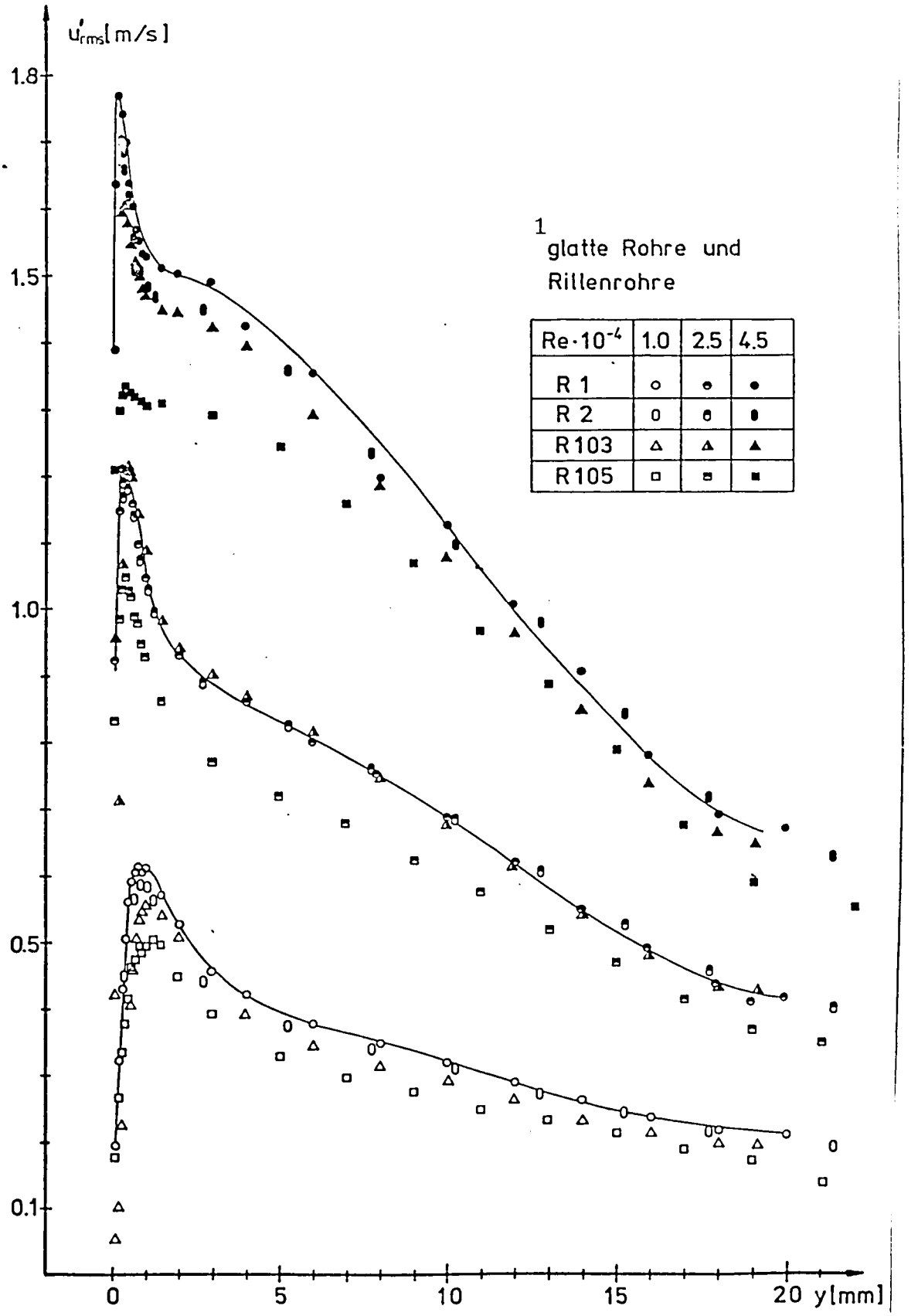

Fig. 5/13: Profiles of Effective Value as a Function of y for 2 Smooth and 2 Grooved Tubes at 3 Reynolds Numbers

Key: 1-smooth tubes and grooved tubes

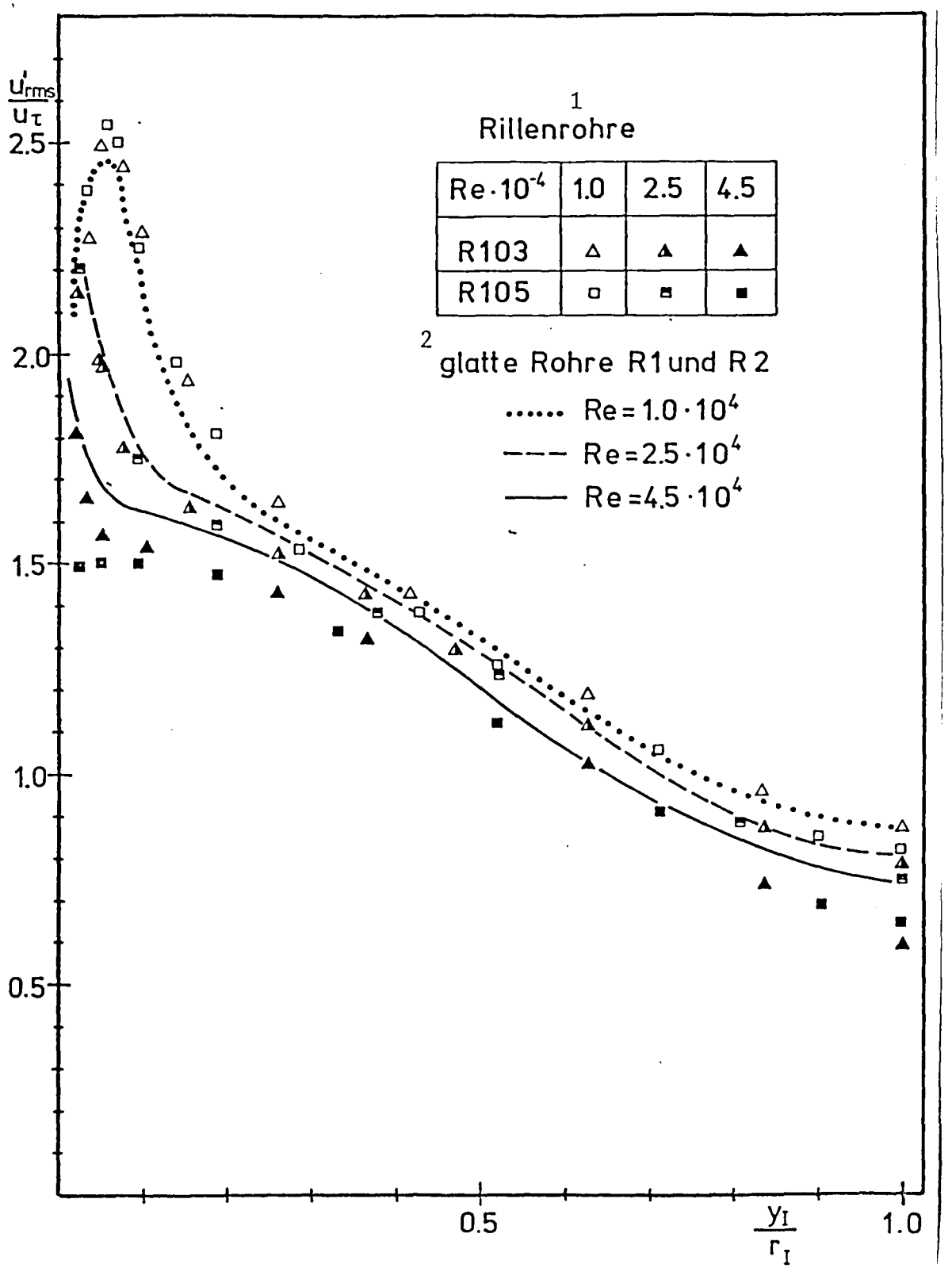

Fig. 5/14: Profiles of Effective Values $\frac{u'_{rms}}{u_\tau}$ for Grooved Tubes R103 and R105.

Key: 1-grooved tubes 2-smooth tubes R1 and R2

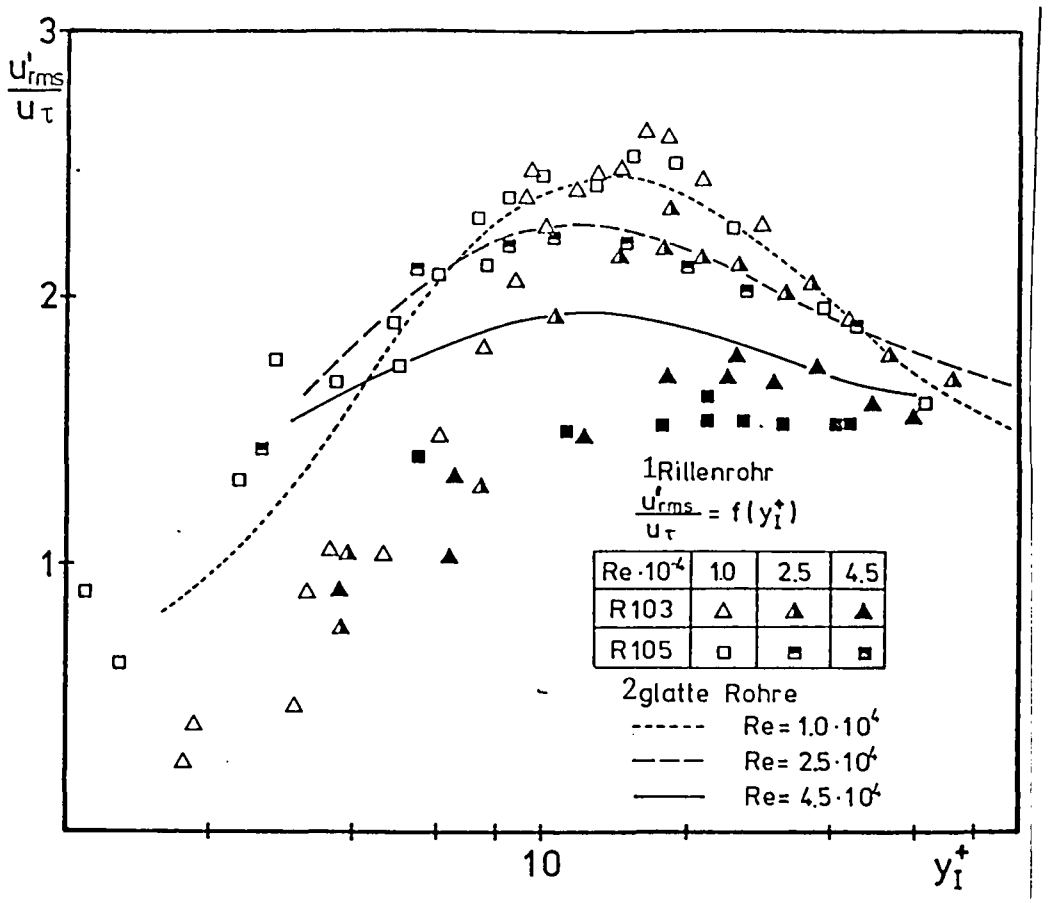

Figure 5/15: Profiles of Effective Values $\frac{u'_{rms}}{u_\tau}$ for Grooved Tubes Near the Wall for 3 Reynolds numbers as Functions of y_I^+.

Key; 1-grooved tube 2-smooth tube

close wall proximity and inaccuracies in positioning. The profiles of effective value were measured and compared with other authors. For Re = $1.0 \cdot 10^4$ a good agreement was obtained, for Re = 2.5 - $4.5 \cdot 10^4$, systematic errors occur due to the non-negligible length of the hot wire. When comparing smooth and grooved tubes, this error plays a minor role. Severe deviations in the velocity profiles and effective-value profiles between smooth and grooved tubes were not found. The profiles coincide within the framework of measurement accuracy on smooth and grooved tubes, if we define the groove crest as the zero point of the y-axis.

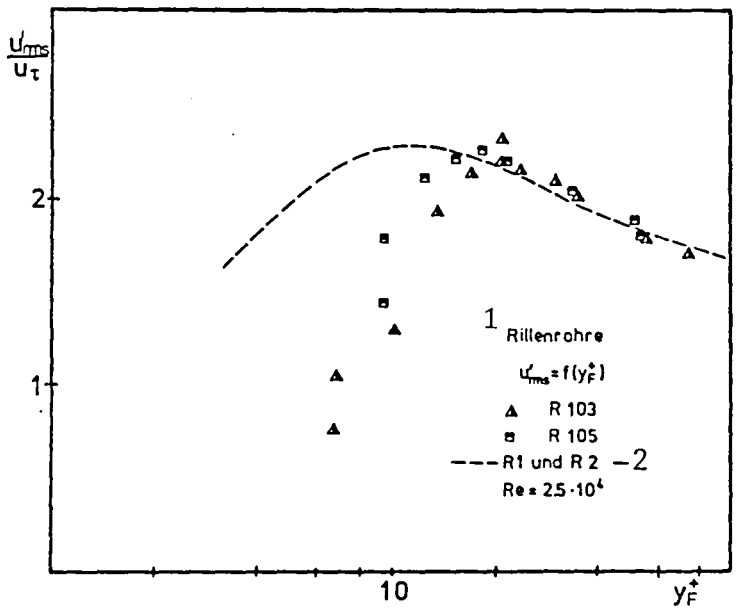

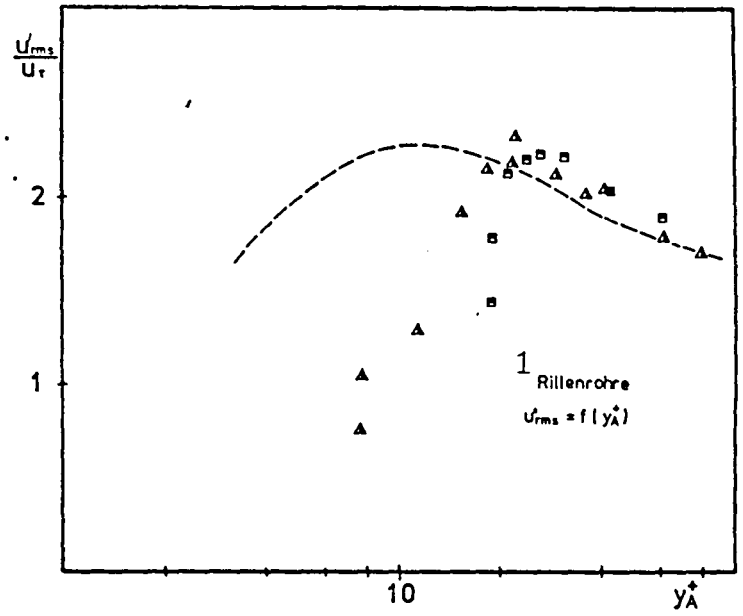

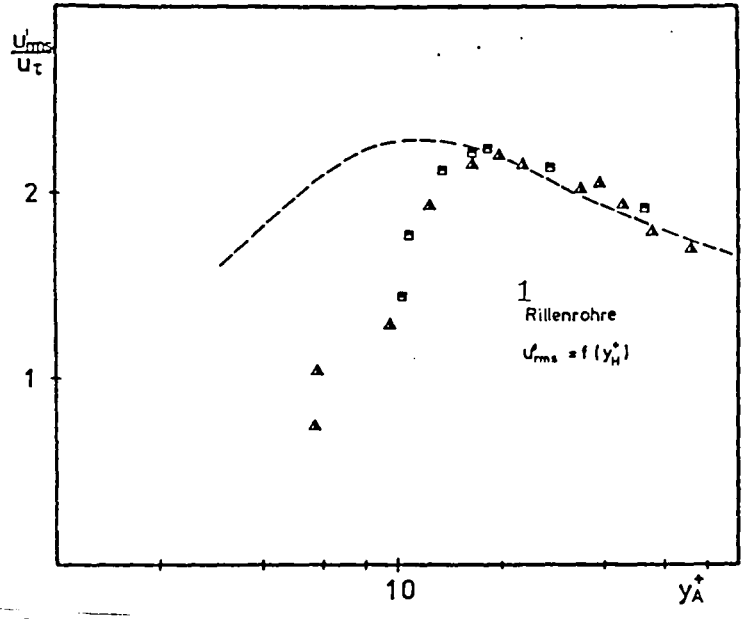

Fig. 5/16: Profiles of Effective Value $\frac{u'_{rms}}{u_\tau}$ for the Near-Wall Grooved Tubes for Re = $2.5 \cdot 10^4$ as a Function of y_F^+, y_H^+ and y_A^+.

Key: 1-grooved tubes 2-R1 and R2

6. Summary and Discussion of Future Work

Under the stimulus of longitudinal grooves discovered by Reif on Shark scales and by more recent investigations of structures in turbulent boundary layers, a hypothesis was developed that suitable longitudinal grooves reduce the flow resistance of a surface.

To check this hypothesis, the resistance law $\lambda = f(Re)$ was checked by measurements of the well-formed part of a tube flow using two smooth and two grooved tubes. For technical reasons, a precise simulation of the grooves on shark scales was not possible. Therefore, the tests were performed on two tubes of different groove profile and the influence of the profile was tested simultaneously. Both grooved tubes exhibited a reduction in resistance of about 3% compared to the resistance of smooth tube in a region of dimensionless groove width $b^+ = b \cdot \frac{u_\tau}{\nu} = 8 \ldots 30$. For the swimming shark, b^+ also lies in this region.

In the second part of this work, the profiles of the average velocity $\bar{u}$ and of the effective value of the velocity fluctuations u'_{rms} were investigated with a hot-wire probe (length of hot wire 1.3 mm 3b). With this measurement method, no large quantitative differences were found between smooth and grooved tubes. By means of a comparison of both profiles of smooth and grooved tubes it turned out that grooved tubes have the same profiles as smooth ones whose interior surfaces lie on the groove crests.

In order to reinforce the results of the first part, additional work could be aimed at changing the groove width b and checking to see whether the region of reduced resistance $b^+ = 8 - 30$ is retained. The result of the second part poses the question of what motion processes take place in the grooves. Future work in this regard could be an investigation of tubes or surfaces with larger grooves in which the flow is examined by hot wires, optical methods or by making the flow visible. A third possibility would be to investigate the influence of grooves on an evolving boundary layer in the tube inlet or at the plate boundary layer.

7. References

Becker, E.: Technical Flow Theory, B.G. Teubner, Stuttgart 1974

Blackwelder, R. and Eckelmann, H.: Streamwise vortices associated with the bursting phenomenon, J. Fluid Mech. 1979, V. 94, part 3, pp. 577-594.

Blasius, H.: The Similarity Law of Friction Processes in Fluids, Research Work in the Area of Engineering, No. 131, Berlin 1913.

Franklin, R.E., Wallace, J.M.: Absolute Measurement of Statis-Hole Error Using Flush Transducers, J. Fluid Mech. 1970, V. 42, part 1, pp. 33-48.

Fromm, K.: Flow Resistance in Rough Tubes, ZAMM 3, 339-358, 1923.

Graichen, K.: Hot Wire Measurements near a Solid Wall, Academy of Sciences of the GDR, Central Institute for Mathematics and Mechanics, Berlin 1980.

Hefner, J.N., Weinstein, L.M., Bushwell, D.M.: A Large Eddy Breakup Scheme for Turbulent Viscous Drag Reduction, Viscous Flow Drag Reduction; Progress in Astronautics and Aeronautics, V. 72, Gary R. Hough editor 1980.

Hofbauer, M.: Visual and Anemometric Investigation of Coherent Structures in the Velocity Field of a Pronounced Turbulent Channel Flow. Reports from the MPI for Flow Research and the Aerodynamic Test Institute, 1978, no. 33.

Hopf, L.: Measurement of Hydraulic Roughness, ZAMM 3, p. 329-339, 1923.

Kirsten, H.: Experimental Investigation of the Development of a Velocity Distribution of Turbulent Tube Flow, Diss. Leipzig 1927.

Kline, S.J., Reynolds, W.C., Schraub, F.A., Runstadler, P.W.: The Structure of Turbulent Boundary Layers, J. Fluid Mech. 1967, V. 30, part 4, pp. 741-773.

Kreplin, H.P.: Experimental Investigation of Longitudinal Fluctuations and Wall-Parallel Lateral Fluctuations in Velocity in a Turbulent Channel Flow. Report from the MPI (Max Planck Institute) for Flow Research and the Aerodynamic Test Institute 1976, no. 63.

Kreyszig, E.: Statistical Methods and Their Application, Vandenhoeck Ruprecht, Göttingen 1977, p. 270f.

Landolt-Börnstein: Numerical Values and Functions from Physics, Chemistry, Astronomy, Geophysics and Technology, V. 4, Technology, Part 1, p. 604, Springer Pub., Berlin, Göttingen, Heidelberg 1955.

Langeheineken, Th.: Relationships between Wall Pressure and Velocity Fluctuations. Reports from the MPI for Flow Research and the Aerodynamic Test Institute 1981, no. 70.

Laufer, J.: The Structure of Turbulence in Fully Developed Pipe Flow NACA Report 1174, 1955.

Laufer, J.: New Trends in Experimental Turbulence Research. Annual Review of Fluid Mechanics, V. 7, p. 307-326, 1975.

Lawn, C.J.: The Determination of the Rate of Dissipation in Turbulent Pipe Flow, J. Fluid Mech. 1971, V. 48, part 3, pp. 477-505.

Nikuradse, J.: Regularity of Turbulent Flow in Smooth Tubes. Research Work in the Engineering Field, no. 356, 1932.

Oka, S.: Influence of Wall Proximity on Hot-wire Velocity Measurements, DISA Information 13, 1972, p. 39-33 [sic].

Pölzin, J.: Measurement of Static Pressure on Rough Walls, Ingenieur Archiv 10, p. 326-338, Springer Pub., Berlin 1939.

Prandtl, L.: Oswatitsch, K., Wieghardt, K.: Führer durch die Strömungslehre [Flow Theory], Friedrich Vieweg & Sohn, Braunschweig, 7th ed. 1969.

Reichardt, H.: Regularities of Straight-line Turbulent Couette Flow, Reports from the MPI for Flow Research and the Aerodynamic Test Institute 1959, no. 22.

Reif, W.E.: Protective and Hydrodynamic Function of the Dermal Skeleton of Elasmobranchs, Neues Jahrbuch für Geologie und Paläontologie, Report 1976-1978, Sonderforschungsbereigh 53, E. Schweizerbart'sche Verlagsbuchhandlung Nägele und Obermüller, Stuttgart 1978, p. 133-142.

Reif, W.E., Dinkelacker, A.: Hydrodynamic Significance of the Squamation of Fast Swimming Sharks, 1981 report 1979-1981 of the Sonderforschungsbereich 53 "Palökologie" Tübingen pp. 494-499.

Rotta, J.C.: Turbulent Flows [Turbulente Strömungen], B.G. Tuebner Stuttgart 1972.

Schildknecht, M.: Experiments on the Influence of Suction on a Pronounced Tube Flow. MPI Report 3/1975.

Schlichting, H.: Experimental Investigations on the Roughness Problem, Ingenieur Archiv 7, p. 1-34, 1936.

Acknowledgement

Thanks to Dr. E.A. Müller for providing the opportunity to perform this work at the Max-Planck Institute for Flow Research. Special thanks to Dr. A. Dinkelacker for suggesting the topic and for his constant readiness to provide valuable assistance, and to Dr. Th. Langeheineken for invaluable discussion of occurring questions and for reviewing the manuscript together with Dr. Borner. Mr. Christmann provided the measurement electronics and numerous technical advice. The director of the mechanical workshops, Mr. H. Hamann quickly put the pipe channel system together and Mr. G. Majewski provided valuable assistance in additional technical efforts and produced the illustrations. Thanks also to Ms. C. Köneke for preparing the manuscript.

End of Document